The Variety of Spontaneously Generated Tropical Precipitation Patterns found in APE Results

Kensuke NAKAJIMA

Faculty of Sciences, Kyushu University, Fukuoka, Japan

and

Yukiko YAMADA

Faculty of Sciences, Hokkaido University, Sapporo, Japan

and

Yoshiyuki O. TAKAHASHI

Center for Planetary Sciences, Kobe, Japan
Kobe University, Kobe, Japan

and

Masaki ISHIWATARI

Faculty of Sciences, Hokkaido University, Sapporo, Japan

and

Wataru OHFUCHI

Earth Simulator Center, Japan Agency of Marine Science and Technology, Yokohama, Japan

and

Yoshi-Yuki HAYASHI

Center for Planetary Sciences, Kobe, Japan
Kobe University, Kobe, Japan

October 31, 2011

Corresponding author: Kensuke Nakajima, Faculty of Sciences, Kyushu University, 6-10-1, Hakozaki, Fukuoka, Fukuoka 812-8581, Japan.
E-mail: kensuke@geo.kyushu-u.ac.jp

Abstract

We examin the results of the Aqua Planet Experiment project focusing mainly on the structure of equatorial precipitation in the subset of participating models on which details of model variables are available. In spite of the unified set-up of APE, the Hovmëllor plots of the precipitation in the models exhibit wide range of diversity, presumably resulting from the diversity among implementations of various physical processes in participating models. Still, the wavenumber frequency spectra of precipitation exhibit certain degree of similarity; the power spectra can be divided into Kelvin mode, westward inertio gravity mode, and "advective" component. The intensity of each of the three components vary significantly in different models. The sum of the variance of the three components reflects, to certain extent, the amount of precipitation on the equator in each of the models, but relative contribution of each components differ among the models. Composite spatial structure of the above three components are made by the space-time filtering to separate each of the three spectral components and performing regression analysis. The composite horizontal structures of Kelvin and westward inertio gravity components in the models are similar to each others and resemble to those expected from corresponding shallow water equatorial wave modes, but the similarity degrades at the levels where the phase velocity is near the zonal mean zonal wind. The horizontal struc-

tures of “advective” components diverge significantly among models. The composite vertical structures for all of the three components are found to be strongly model dependent. Based on the comparison among vertical and horizontal structure of convective and stratiform heating in the composite disturbances, the diversity of vertical structure originates from the difference in physical processes, implementation of cumulus parameterization in particular.

1. Introduction

Convective activity in the earth's tropical atmosphere is recognized to exhibit a hierarchical structure including individual cumulonimbi, mesoscale features, cloud clusters (Houze and Betts 1981), various kinds of synoptic scale disturbances such as convectively coupled equatorial waves (Kiladis et al. 2009), intraseasonal variability (ISV) (Madden and Julian 1972), and climatological features like intertropical convergence zone (ITCZ) or convection centers. Each of the classes in the hierarchy has unique importance, for example in the role in the maintainance of the climate system (Sherwood et al. 2010), predictability of the numerical weather prediction, or severe meteorological phenomena central to the disaster prevention. Thus, the reproduction and the understanding of the hierarchy is one of the most important theme of tropical meteorology.

There remains a large degree of difficulty in our efforts to capture the hierarchical structure. The most obvious difficulty is its extremely wide range of spatial and temporal scales; there is four orders of magnitude difference from the smallest member, individual cumulonimbi having 1–10 km scale, to the largest member, ISV and ITCZ, which have a global scale. If we wish to simulate whole of the hierarchical structure explicitly, we have to run a global cumulus resolving model; its execution requires huge computational resource (Tao and Moncrieff 2009). Up to present, only a very limited number of such explicit calculations are accomplished (Satoh et al. 2008). Other than such explicit simulations, any kinds of global modeling is, to more or less degree, compromised to incorporate the effect of the smaller classes of the hierarchy, i.e., cumulonimbi and mesoscale systems. The most common way of the compromise has been to employ cumulus parameterization, although there are a few exceptional attempts to avoid cumulus parameterization by using "distorted" dynamical equations (Kuang et al. 2005).

It is true that computational resources are rapidly developing, some degree of cumulus parameterization is considered to remain in global models at least for long term runs for the projection of possible global warming. Therefore, the knowledge on the performance of the numerical models employing cumulus parameterizations in the reproduction of tropical convection hierarchy remains important in some unforeseeable period in the future. At present, there are not small number of cumulus parameterization used in operational or community atmospheric models including adjustment type schemes (Manabe et al. 1965), mass flux schemes (Tiedtke 1989), and the schemes employing ensemble of cumulus (Arakawa and Schubert 1974). In spite that each of the numerical models are highly tuned to reproduce the behavior of the real atmosphere when used in the atmospheric models, it has been known that properties of tropical atmospheric convection in numerical models exhibit wide variety, and it is still agreed that no single model can be nominated as the one that reproduce the reality. We have to examine how and why various models behave differently by comparing the results of such models in a common setup in inter comparison comparison projects such as AMIP or CMIP.

Aqua-planet experiment project (APE) is an attempt to compare the behavior of modern sophisticated numerical models used for numerical weather prediction or climate simulations in the simplest set-up of the "aqua planet", i.e. a virtual planet wholly covered with ocean of fixed surface temperature. The context and aim of the APE is fully discussed in Blackburn and Hoskins (2011), where the history and the position of idealized AGCM experiments in the framework of atmospheric research in general is also stated. The setup of aqua-planet was first employed purposefully by Hayashi and Sumi (1986) in order to find the "natural" behavior of tropical atmospheric convection with a successfully identifying the hierarchy, or its substitutes in low resolution model employing cumulus parameterization, suggesting cloud clusters, super cloud clusters, ISV, tropical cyclones and double ITCZ. One may regard this setup is trivial or easy one because it is free from complex treatment of land surface and associated hydrology and/or vegetation schemes. Still, it presents a unique and difficult challenge to AGCMs; being free from the external forcing provided from the inhomogeneity of underlying surface, the model atmosphere have to determine its behavior by itself, so that both of the strength and the weakness of each numerical models would be exposed clearly. In fact, as early as at the begging of 1990's, it has been clarified the choice of cumulus parameterization strongly affects several fundamental properties of AGCM such as the behaviors of tropical disturbances (Numaguti and Hayashi 1991a) or the structure of ITCZ (Numaguti and Hayashi 1991b).

The present paper describes the behavior of equatorial precipitation structure in CONTROL experiments conducted in APE project. Among the series of classes of the hierarchical structure of tropical precipitation convection, we will focus our attention to the "intermediate" scale structure, i.e., convectively coupled equatorial waves (Kiladis et al. 2009), because of the following reasons in particular. First, which is the most trivial reason, the smaller classes, individual cumulonimbi and mesoscale systems are below the resolvable scales of most of the AGCMs participating the APE project. Second, which is also trivial, the larger classes, ISV and larger scale, are presumably strongly affected by the present idealized, unrealistic setup of aqua planet, so that the behavior of the models are not expected to be tuned well. It is also possible that mechanism governing ISV in the present setup is different from the ISV in the real atmosphere, so that these features should be examined from a wider perspective elsewhere. Third, which is the most important, is that, as will be shown later, the behavior of convectively coupled waves in the models in APE displays rich variety possibly depending on the choice of cumulus parameterization employed. The examination of variety of the properties of CCEWs in APE should enhance our knowledge on the underlying mechanism governing the CCEWs in coarse resolution AGCMs, which would lead us to the guiding principles on how to tune cumulus parameterization so as to better represent the behavior of the real atmosphere.

The paper is organized as follows. Section 2 will explain the setup of experiment. Because details of the APE project is given elsewhere (Blackburn and Hoskins,2011), only brief summary will be presented. Section 3 will present the method of analysis. Section 4 will compare gross feature of CCEWs in APE models. Section 5 will compare the composite structure of three categories of CCEWs produced from the regression analysis of spectrally filtered time series from several selected models participating the APE project. Discussions and conclusions will be given in the last two sections.

2. Setup of Experiments

The experiments to be examined in this paper is the CONTROL case of the APE project. For the details not touched here, readers are referred to the context paper (Blackburn and Hoskions 2011) or the original proposal paper (Neale and Hoskins 2000). The SST distribution is zonally uniform and fixed in time. The meridional structure is shown in Fig. 1. The SST profile is characterized with a rather sharp single peak located at the equator and north-south symmetric. The latitudinal gradient in steep from subtropics to midlatitude, whereas it flattens in high latitude region. Reflecting this character, climatological subtropical and mid-latitude jets effectively merge to form a single very strong jet located in subtropics.

In the APE project archive, the results of 17 AGCM runs from 15 groups are accumulated. A brief summary of the specification of the models is given in Table 1. Among these, 7 groups provided more detailed time series on additional model variables for 8 runs, from which we obtain composite structure as presented later. It is worth mentioned that even the subgroup on which composite analysis is made contains wide variety of spatial resolution and cumulus parameterizations employed. More complete specifications are given in the APE-ATLAS (Williamson et al. 2011) to which readers are referred to. Table 1

Fig. 1

3. Methods of analysis

3.1 Data

The primary data used in this study are the 6-hourly one year time series ("TR") of CONTROL experiments. We also analyze the "additional transient time series" containing multilevel model variables in 7 AGCM runs conducted in the APE project, which are AGUforAPE, CSIRO_std, ECMWF05, ECMWF07, GSFC, LASG, NCAR. In the present paper, we mainly examine on the latter data. The former contains model variables on very limited model levels, and are only consulted in order to check the representativeness of the 7 model runs focused in this study among all of the AGCM runs. The variable we examined are eastward wind, northward wind, vertical velocity, temperature, geopotential height, specific humidity, and, precipitation flux. In addition, temperature tendency due to parameterized convective process and that due to resolved condensation are used in the composite analysis of disturbances. Note that the temperature tendency terms are not provided for CSIRO_std, and LASG does not provide the tendency due to resolved scale condensation.

3.2 Hovmëllor plots and wavenumber frequency spectra

In section 4, we show plots of time evolution ("Hovmëllor" plots) and wavenumber frequency power spectra.of precipitation along the equator. The former is produced simply by extracting the precipitation on the equator; for the models that do not have grid points on the equator, the data at the grid points in southern hemisphere nearest to the equator is used instead. The wavenumber frequency spectra.are made by the following procedures. (i) From the original 1-year time series of each model run, ten 90-day time series are made which begin at every 30 days from the beginning. (ii) From each of the 90-day segment, linear trend, which is estimated using least square fit, is subtracted. (iii) Double Fourier transform is executed to obtain the space time power spectrum of each of the segments. (iv) All of the space time power spectra of the ten 90-day segments are averaged to obtain the final estimates of the wavenumber frequency power spectrum of the precipitation in the model.

In addition to the wavenumber frequency power spectra, we present the "enhanced" power spectra of the meridionally symmetric component of precipitation within 5 degree latitudes. The methods to obtain the enhanced spectra basically follows that used in Wheeler and Kiladis (1999). (i) The time series of north-south symmetric component of precipitation is made at each latitudes. (ii) The wavenumber frequency power spectra of the above time series is made in the same procedure as explained in the previous paragraph for the power spectra at the equator. (iii) Thus obtained power spectra at all latitudes within 5 degree from the equator are averaged. (iv) The above spectra are divided by their "background" spectra, which are obtained by applying 1-2-1 smoothing in wavenumber and frequency 40 times.

3.3 Wave-type filtering

In section 5, we examine the structure of disturbances associated with the precipitation at the equator separating the types of the convectively coupled equatorial disturbances. The method of separation basically follows that in Wheeler et al (2000). We focus on three types of convectively coupled equatorial disturbances, which are Kelvin (n=-1)mode, westward inertio gravity (n=1) mode, and "advective" component. (Hereafter these three components are referred to as K mode, WIG mode, and AD components, respectively.) The last one has been referred to as "TD-type" component in Wheeler and Kiladis (1999). However, the ITCZ appearing in the CONTROL experiment in most models are sharply concentrated at the equator (Blackburn et al. 2011a), so that the disturnabce in the wavenumber frequency domain of the traditionally called "TD-type" do not necessarily accompany vorticity which is an important character of conventional tropical depressions, so that we choose the name of "advective component" instead.

The procedure to isolate each of the three types of components again basically follows that of Wheeler et al (2000). (i) We perform double Fourier transformation of the three dimensional time series of the variables to be analyzed in longitude and time. (ii) We filter the wavenumber frequency spectral coefficients that passes each of the wavenumber frequency domains that characterize the three types of disturbances, whose specifications are described below. (iii) We perform inverse double Fourier transformation of the filtered wavenumber frequency to obtain the three dimensional time series of variables representing each of the three types of disturbances. The definitions of the filters for the three disturbance types are shown in Fig. 2. The range of equivalent depth associated with the K filter is broader than that in Wheeler and Kiladis (1999). where the range between 8m and 50m is employed. By the present choice, we intend to cover the wide variety of Kelvin wave type disturbances appearing in the APE experiments. In each of the experiments, however, the range of the equivalent depth of dominant Kelvin component is much narrower, as will be presented later.

3.4 Composite structure

In Section 5, we present composite structure of K, WIG, and AD components along equator appearing in each of the seven AGCM runs. The composite structure is obtained by performing (simultaneous) regression analysis of the time series of model variables filtered through one of K, WIG or AD filter. Thanks to the idealized zonally symmetric configuration of the CONTROL experiment of APE, the procedure of regression is quite simple. We extract a time series of a filtered model variable (*predictand*) at a height and a latitude, and shift the extracted data longitudinally by a certain zonal length, and calculate the slope of linear regression of the shifted time-longitude data against filtered precipitation at the equator. For models that does not have grid points at the equator, the average of the precipitation along the two latitudes are used instead. By repeating this procedure for all latitude, height, and zonal shift length, we can obtain the composite three-dimensional structure of the model variable for the disturbance of the filter used. We will not perform the lagged regression analysis, but averaged temporal evolution of the disturbance is, to some extent, expected to represented as the zonal structure of the composite disturbance. The detail of the temporal evolution may be of interest, but it is left for future research.

It should be bear in mind that the magnitude of the regression slope of a particular variable at certain position for a particular model does not necessarily represent the intensity of the model variable actually realized in the model; it depends on the intensity of the filtered rainrate along the equator realized in the model, which varies significantly on different models as will be shown shortly below. The units of the regression slope are the units of the predictand per unit rainrate. However, for convenience, we multiply the values of the regression slope by a normalization intensity of precipitation, which is 0.0001 $[kg \cdot s^{-1} \cdot m^{-2}]$, and represent all predictand with their original units. Fig. 2

4. Behavior of equatorial precipitation in APE models

4.1 Hovmëllor plot of equatorial precipitation Fig. 3

Fig. 4

Fig. 5

Temporal evolution of precipitation at the equator of each model is shown in Fig. 3, where one can find quite a wide range of variety among the hierarchical structure of precipitation in different model runs. The structure seem to depends equally on the parameterizations of physical processes and on the spatial resolution. For example, higher resolution models such as DWD, ECMWF, FRCFC, CSISRO represents fine spatial structure, which lacks in lower resolution models, such as AGUforAPE, CGAM etc. On the other hand, the behavior of ECMWF_05 and ECMWF_07, which has the same resolution and slightly different cumulus parameterization, differ considerably. The variety represented by all APE models is so widespread that is difficult to describe meaningfully how one model differs from another. So we only point out several noteworthy features.

In some models, eastward propagating planetary scale signals, whose propagation speed is not very different from ISV in the real atmosphere (Madden and Julian 1994), are notable with different intensity. FRCGC, i.e., NICAM run shows most prominent eastward propagating signal as was described in Miura et al (2005) and Nasuno et al (2008). It is also evident in the results of K1Japan, two versions of UKMO, and two versions of ECMWF, but the intensity or detailed structure differ considerably. On the other hand, such eastward propagating low wavenumber signal is weak or absent in AGUforAPE, NCAR, and CISRO-old. In spite that these models are common in lacking notable eastward propagating signal, they differ significantly; the precipitation in NCAR is generally weak and rather uniform, whereas that in CISRO-old is generally intense, and that in AGUforAPE are organized in westward propagating structure.

If we focus on smaller scale structure, as a common feature, precipitation occurs near the "grid scale", i.e. nearly smallest scale resolvable in all models, but the behavior of the grid scale precipitation varies significantly. The life time of such grid-scale precipitation varies among models ranging from about one day to nearly ten days. Moreover the direction of migration of those gridscale precipitation structure also differ among models: those in AGUforAPE and MIT move generally westward, those in ECMWF-05 and GFDL are nearly stationary, and those in UKMO, K1JAPAN, ECMWF-07, DWD, and CSIRO move generally eastward.

4.2 Space time spectra of precipitation

In contrast to the extremely rich variety in the appearance of equatorial precipitation in longitude time plot, the wavenumber-frequency spectra of the equatorial precipitation of 17 model runs (Fig. 4) exhibit some degree of similarity. The most common feature is the eastward propagating signal. In most model, the dominant power of the eastward propagating signal is distributed mainly along respective dispersion relation of Kelvin mode, although the intensity, characteristic equivalent depth, and, dominant zonal wavenumber differ among the models. The identification of these signal as the Kelvin mode is supported by the composite analysis of its spatial structure, which will be shown later.

The eastward propagating signal in NCAR is, however, somewhat different from those in other models; the dominant wavenumber, 5–10, is much larger than that in other models, 1–5. Moreover, the strong power seems to be distributed along the dispersion curve of n=1 eastward propagating inertio gravity wave (EIG). Strangely, the wavenumber-frequency spectrum of mid-tropospheric vertical velocity (not shown) exhibits much weaker wavenumber dependence, so that the ratio of the intensity of precipitation to the intensity of vertical velocity, which might be interpreted as the gross sensitivity of the response of the latent heating to the grid scale ascent, strongly depends on the wavenumber; precipitation is much mode sensitive to vertical velocity in zonal wavenumber 5–10 than in zonal wavenumber 1–5. In the results of other models, there are not such distinct variation of the sensitivity, and their magnitude are more or less similar to that for the wavenumber 5–10 in NCAR. It should be also noted that the reduced "sensitivity" of precipitation to the vertical velocity in NCAR is observed only near the equator. This latitudinal dependence may be related to the latitudinal profile of ITCZ; NCAR is characterized with distinct "double ITCZ" structure, but most of other models in APE is characterized with "single ITCZ". These evidence suggest that the eastward propagating signal in NCAR bear some character of eastward propagating inertio gravity wave with equivalent depth is about 12 m. However, as will be shown later, its structure is not very different from that of Kelvin wave.

In contrast to the more or less common emergence of Kelvin signal, the intensity and the spreadings of "background component" vary much more drastically among the models. They reflect both the climatological structure of ITCZ and the structure of precipitation events. As is described in Blackburn et al (2011a) the mean precipitation intensity at the equator varies over a factor of 3 among the models, and, as will be shown in the next section, the model with larger mean precipitation intensity exhibits the larger power of over-all variance of precipitation. The frequency and wavenumber bandwidths are, from the definition of the Fourier components, related to the degree of concentration of precipitation in the real space. More widespread background component found in DWD, ECMWF05, LASG, and NICAM reflect more concentrated grid-scale precipitation structure noted in fig. 3. It is interesting that, in most models, westward component extends to higher frequency than eastward component does, although the reasons are unclear.

More intricate features are more easily seen in fig. 5, which are produced after the signal enhancing technique of Wheeler and Kiladis (1999). The westward propagating background component, are, in some models, divided into the component along the dispersion curve of westward propagating inertio gravity wave and component of lower frequency. The former will be called “inertio gravity wave’, or WIG, component, following the notation used for observed OLR in Weeler and Kiladis (1999). The latter components will be called “advective” components because they are generally distributed about straight lines passing through the origin in the frequency wavenumber space, so that the motion appear to result from the advection caused by certain easterly wind, although the actual relationship between the propagation speed of the advective components and the zonal wind is not straight forward as will be discussed later.

The behavior of WIG signals exhibits significant variety among models, although to smaller degree than for the advective components. In AGU-forAPE and CGAM, the WIG signal is very weak, while it is distinct in LASG and K1JAPAN. Not only the intensity but also the distribution over the wavenumber-frequency space varies: the signal covers a wide range of wavenumber in LASG and K1JAPAN, but only higher wavenumber component can be noted in GSFC. It is worth noting that there is a gradual change of the characteristic equivalent depth of WIG as wavenumber varies: the WIG of larger scale has the shallower equivalent depth. The most clear example is that in LASG. This tendency may suggest that the strength of the coupling between the modelled convective heating and the large scale convergence associated with the WIG depends on the wave period resulting in the varying degree of "reduced stability" effect discussed by Gill (1982).

Because of the clean setup of the aqua planet experiment project, one can also note several types of planetary scale disturbances. other than the convectively coupled equatorial waves and advective signals. One is the quasi-stationary wavenumber five signal. Most prominent example can be found in the result of NCAR. Together with ten-day period wavenumber six component nearby, it seems to be associated with the midlatitude baroclinically unstable waves like those examined by Zappa et al (2011). Another type of examples are the diurnal and semi-diurnal migrating tides (Woolnough et al. 2004). Additionally, several types of normal mode waves, which are the 33-h Kelvin wave (Matthews and Madden 2000), the mixed-Rossby gravity mode, $n = 0$, and Rossby modes, $n > 1$, (Hendon and Wheeler 2008) for their counterparts in the real atmosphere, can be found. These features are only marginally identifiable in the space-time spectra of precipitation, but are more easily confirmed in the spectra of zonal wind or surface pressure (not shown here). Among these waves, the representation of the 33-h Kelvin wave is found to be sensitive to the vertical resolution and/or upper boundary conditions of the models, although other type of planetary scale disturbances mentioned above are more insensitive. The description of those waves is left for future research.

In many experiments, the tidal signal modulates the tropical precipitation associated with the Kelvin or advective signals significantly. Such modulation results in high frequency, low wavenumber component that sometimes overlaps the frequency-wavenumber domain of WIG and/or EIG(Eastward propagating Inertio Gravity wave). Most clear example is the branch going through (wavenumber,frequency)=(-5,0.9) and (-10,0.6) in the spectra of

UKMO (fig. 5(p,q)).

5. Spectral filtering analysis

As described in the previous section, there are prominent variety in the space-time structure of equatorial precipitation in APE models. It it highly probable that various different choice of discretization schemes, spatial resolution, and parameterizations of physical processes among the models result in the variety of model behavior. However, it is quite difficult task to point out one or more items that cause one or more particular difference of behavior. Before any progress be made, it is necessary to describe the difference of model behavior.

As an attempt to systematically describe the varying behavior of equatorial precipitation in the APE models, we separate the model variables into the contributions of Kelvin, WIG, and advective components, then construct composite structure of them for each model, and compare the character of each composite waves in various models.

The experiments to be analyzed are CONTROL cases done by the subset of APE models, of which the detailed transient datasets are submitted, which are AGUforAPE, CSIRO, ECMWF-05, ECMWF-07, GSFC, LASG, and NCAR. In spite that the spectral property of each component differ among models, we use the same definition for the filters to extract each of the three spectral components, which are shown in Fig. 2. As a result, some part of the dominant spectral power is excluded from the composite in some models, the most significant of which is the low wavenumber part of the WIG in LASG. By this choice, we prioritize the uniformity of filters applied to the results in all of the models to be compared than the completeness of coverage of the three spectral components appearing in the models.

5.1 Intensity of Kelvin, gravity and advective components

Fig. 6

Fig. 7

Before examining the spatial structure of each components, we compare their intensity in the APE models. Fig. 6(a) shows the variance of equatorial precipitation calculated from the time series that are filtered by K, WIG, and AD filters in the seven APE models. It is found that the intensity of all components are strongly model dependent. LASG and ECMWF05 are members that exhibit strongest disturbances, whereas NCAR, GSFC, and CSIRO are those with weakest. All of the Kelvin, gravity, and advective components summed up, the intensity in ECMWF05 is about 6 times as large as that in NCAR. The significant difference of intensity of disturbance in the model can be mostly explained by the difference of rainfall intensity at the equator. Fig. 7 is the scatter plot showing the relationship between squared time mean zonal mean precipitation intensity at the equator and the overall intensity of disturbance, which is defined as the sum of the three components. Total variance, i.e., the variance of unfiltered precipitation at the equator, are also plotted for the corresponding model. We can find that both the overall disturbance intensity and the total variance are well correlated to the average precipitation intensity squared. There are two outliers; LASG exhibits larger variance, whereas CISRO exhibits smaller variance. Lastly, we examine the relative contribution of the three disturbance components to the variance of precipitation. Fig. 6(b) compares the variance of Kelvin wave, gravity wave, and advective components scaled by the total variance in each of the models. Two aspects can be commonly noted for all of the models; the sum of the three components contributes about half or larger part of the total variance, and the gravity wave component is weakest in the three kind of disturbances. However, the relative contributions of Kelvin wave and advective components varies largely. There is weak negative correlation between the intensities of Kelvin wave and advective components. AGUforAPE and ECMWF07 show contrasting feature; advective components dominates in AGUforAPE, whereas Kelvin wave dominates in ECMWF07. How the contributions of the three components are determined in each model is very important issue. We next examine the structure of the Kelvin wave, gravity wave, and advective components appearing in each of the model in the next subsection, hoping that the analysis may provide clues to the above mentioned issue.

5.2 Composite structure of Convectively Coupled Equatorial Waves

Hereafter, composite structure of Kelvin wave, westward gravity wave, and advective component filtered structure of the seven APE models. As was written in section 3, the composite structure is derived from the regression of corresponding filtered variables to the symmetric component of filtered precipitation intensity at the equator. The variables in the following figures are scaled for $0.0001[Kg/s \cdot m^2]$ precipitation anomaly at the reference latitude, 180 degree longitude, so that the intensity of composite disturbance presented in the following figures do not represent the intensity of those disturbance emerging in the models; only the structure matters.

a. Kelvin filtered component

Fig. 8 Fig. 9 Fig. 10 Fig. 11 Fig. 12 Fig. 13 Fig. 14

Composite Kelvin wave mode is presented in Fig. 8–14. Fig. 8 shows the horizontal structure of precipitation and horizontal wind on 925hPa for the K filtered composite. In all models, the precipitation anomaly is well confined near the equator. However, the latitudinal extent somewhat differ; They are sharply confined to the equator in EC05 and LASG, whereas they are broad in AGU, EC07, and NCAR. Generally, the north-south extent correspond to the width of the ITCZ in each model (Williamson et al. 2011). The longitudinal structure also differ among the models; it is confined in

LASG and EC05 and GSFC, and is broader in AGU and EC07. In NCAR, the precipitation anomaly has a wave-like variation with the wavelength of 2500–3000km, and associated with off-equatorial component which is delayed with 10 degrees. Similar off-equatorial component can be found also in GSFC. Note that both of the two models are characterized with distinct double ITCZ structure (Williamson et al. 2011). The horizontal wind structures deviate from that expected from the shallow water Kelvin wave (Matsuno 1966) with different degrees; commonly found feature is meridional convergence. It typically occurs at almost the same location of the zonal convergence. The intensity of the meridional flow is not very different from that of the zonal flow.

Fig. 9 shows the horizontal structure of geopotential and horizontal wind on 850hPa surface for the Kelvin wave component. We can observe that, in most of the models, the horizontal structure of the disturbance is similar to that of shallow water equatorial Kelvin wave (Matsuno 1966) the geopotential and zonal wind perturbations are positively correlated and confined within several degrees from the equator. Zonal component dominates in the wind field near the equator, converging around the location 5-10 degrees to the east of the maximum precipitation anomaly. As a feature that deviate from the structure of classical shallow water Kelvin wave, we can note the significant meridional wind perturbation near the precipitation maxima.

However, the strength of the meridional wind perturbation depends on the choice of variable for the key used to the regression; composite horizontal structure based on the regression to low level zonal wind at the equator (not shown here) exhibits much weaker meridional wind, displaying larger degree of similarity to the shallow water Kelvin wave.

An apparent exception is AGUforAPE. Around the location of the maximum precipitation anomaly, the the zonal wind perturbation is strongly confined in the vicinity of the equator. One can notice cyclonic curvature of the wind perturbation around 5 degree latitude, which suggests the possible existence of weak Rossby response. It is noted that, the meridional wind perturbation converging around the maximum of precipitation seems to be originating in higher latitude, where we can find a pair of geopotential perturbation, positive to the west and negative to the west, that is, in geostrophy, consistent with the equatorward converging meridional wind perturbation. The Kelvin wave filtered correlation coefficient of the subtropical geopotential perturbation to the equatorial precipitation exceeds 0.15 around the longitude of precipitation maximum, suggesting possible existence of forcing from, or interaction with mid-latitude.

By more careful inspection, we can find that NCAR is another exception. First, while there is only one pair of high and low pressure anomaly along the equator in other models, two or more pairs can be clearly noted in NCAR. This feature is consistent with the character of the power spectra of equatorial precipitation; wavenumber 7–10 component is dominant in NCAR (Fig. 4(o)), whereas smaller wavenumber component is dominant in other models. Second, the precipitation anomaly exhibits a significant meridional phase difference; the zonal maxima in the latitude of the ITCZ is located at about 10 degree to the west of that at the equator. This horseshoe like structure is also interpreted as the superposition of the equatorial Kelvin wave and the eastward inertio gravity wave, the latter being shifted by about 5 degrees to the east of the former. This interpretation is not inconsistent with the structure of low level horizontal wind that deviates from that of pure Kelvin wave. As noted earlier, in NCAR, the eastward propagating precipitation signal in the frequency wavenumber space (Fig. 3(o)) seems to be dominated along the dispersion relation of the eastward inertio gravity wave having the equivalent depth of about 10 m. These two evidence suggests that, the eastward propagating equatorial precipitation structure in NCAR includes, in addition to the conventional equatorial Kelvin wave structure, some contribution of eastward propagating inertio gravity wave.

In contrast to the above mentioned similarity in the low level structure, considerable model dependence can be found in the upper tropospheric structure. Fig. 10 shows the horizontal structure of geopotential and horizontal wind on 250hPa surface for the Kelvin wave component. Divergence of zonal wind perturbation around maxima of precipitation, which is expected for Kelvin-like disturbance, is found only for LASG and NCAR. In ECMWF07 and GSFC, the area of zonal wind convergence is found far to the east of the precipitation maximum. In AGUforAPE, CSIRO, and, ECMWF05, zonal wind is convergent at the precipitation maxima; the horizontal divergence that is required as the continuation of the upward flow at the precipitation maxima is accounted exclusively by the divergence of meridional flow. Additionally, significant vortical perturbations are notable in the subtropics, although the phase of the vortices relative to the location of the precipitation maxima varies among the models. These diversity of upper troposphere appear because the phase velocity of the Kelvin wave like perturbation, which is typically $10 \sim 30$ m/s, is not very different from the zonal mean zonal wind in the upper troposphere in the tropical to subtropical latitude in the models, so that Rossby wave like response can be resonantly excited, and the structure of the response could be sensitive to the subtle difference of the structure of basic state and the heating in the precipitation anomaly.

Fig. 11 shows the vertical structure of temperature, zonal wind, and vertical velocity along the equator for the Kelvin wave component. The vertical structure of the Kelvin mode appearing in models displays a wide variety. We can notice at least four types of temperature perturbation among the composite structure in the models. i.e., the first baroclinic mode signal extending whole depth of troposphere, the second baroclinic mode signal which has two maxima of amplitude in the troposphere that are somewhat out-of-phase to each other, the shallow signal at around 600hPa that are presumably associated with the melting of ice phase hydrometeor, and another shallow signal near the surface possibly associated with the evaporation of raindrops. In each of the models, the four types of temperature signal appear in different combination, intensity, and phase relationship, resulting in the wide variety of the temperature structure.

Fig. 12 shows the vertical structure of specific humidity, zonal wind, and vertical velocity along the equator for the Kelvin wave component. As a common feature, in most models, the humidity field is characterized with a "slant" structure; lower troposphere is moist to the east of the rainfall anomaly, and dry to the west, whereas middle and upper troposphere is dry to the east and moist to the west. In GSFC, however, east-west contrast of the humidity is in opposite sign to that in the other models. Another common feature is shallow dry region near the surface to the west of the precipitation anomaly, which presumably results from (parameterized) evaporation of raindrops.

Structure of circulation on the equator, which is shown in Fig. 11 and Fig. 12, considerably vary among the models. In majority of the models, first baroclinic mode structure dominates in the vertical velocity, although the location of upward motion does not necessarily corresponds to the area of upper level zonal divergence because of the significant contribution of meridional divergence as will be shown later. However, some degree of westward tilt, or some contribution of the second baroclinic mode, can also be noted in most models. Clearest examples are found in ECMWF07, LASG, and NCAR. The composite disturbance in GSFC has one notable feature; a significant cool downward flow in the lower troposphere, which is somewhat similar to the mesoscale downward flows that develop below anvil clouds associated with mesoscale precipitation features (Houze and Betts 1981), is found to the west of the maximum of precipitation in GSFC. However, its zonal extent is too broad to be regarded as mesoscale; this feature could be explained as a cumulative effect of more compact cold downdraft found in the advective mode, which will be presented later.

The composite structure of temperature tendencies due to parameterized convection, DTCONV, and that due to resolved clouds, DTCLD, on the equator are shown in Fig. 13 and Fig. 14, respectively. In all models, DTCONV is zonally well confined. In NCAR significant negative value is observed to the west and east of the precipitation anomaly, but, considering that the precipitation itself has a zonally wavy structure (Fig. 13(e)), it corresponds directly to the in situ precipitation. On the other hand, vertical structure of DTCONV strongly model dependent. In LASG, it is distributed mainly in the lower troposphere. In AGUforAPE, EC05, and, EC07, it is mostly confined above the freezing level, whereas in GSFC, NCAR, it has a deep structure extending both lower and upper troposphere. In EC07, there is a region of cooling near the surface, presumably resulting from parameterized rain evaporation.

The structure of DTCLD is strongly model dependent, not only in its vertical structure but also in its zonal structure. In AGUforAPE and EC05, DTCLD is zonally confined and its vertical structure is similar to that of DTCONV in the corresponding model. In EC07, GSFC, and presumably NCAR, DTCLD extends much more extensively in zonal direction than the precipitation. In EC07 and GSFC, the vertical structure has the second baroclinic mode feature; the heating in the lower troposphere is positive to the east and negative to the west of the updraft, nicely representing the cooling due to evaporation of stratiform precipitation. It should be noted that the cooling area extends about 3000 km to the west of the updraft, which is much wider than the typical extent of "mesoscale precipitation features" (Houze and Betts 1981). As a result, overall structure of the heating is somewhat similar to "giant squall lines" observed in the upward motion area of Madden Julian Oscillation as described e.g. in Mapes et al (Mapes et al. 2006). There is also a shallow region of cooling near the surface in EC05, EC07 and NCAR. Such cooling near the surface is absent in AGUforAPE.

In summary, the composite structure of Kelvin filtered component has some degree of similarity to Kelvin waves discussed previously in many aspects. It is especially true for the horizontal structure in the lower troposphere. The vertical structure is shown to be strongly model dependent, and the intensity of the Kelvin component disturbance in particular model seems to be correlated with how much the composite disturbance is similar to the unstable modes of wave-CISK. It should bear in mind, however, that the vertical structure of the heating is, in most models, far from zonally uniform, so that wave-CISK in its classical sense (Hayashi 1970), where cumulus heating is assumed to proportional to the vertical velocity at the top of the boundary layer with fixed vertical profile, does not apply to the composite Kelvin filtered disturbances as it is.

b. Westward propagating gravity wave filtered component

Composite gravity wave mode is presented in Fig. 15–21. Fig. 15 shows the horizontal structure of precipitation and horizontal wind on 925hPa surface for the WIG component. Fig. 16 shows the horizontal structure of geopotential and horizontal wind on 850hPa surface for the gravity wave component. We can observe that the horizontal structure of the pressure

Fig. 15
Fig. 16
Fig. 17
Fig. 18
Fig. 19
Fig. 20
Fig. 21

and wind disturbance is similar to that of shallow water westward propagating equatorial gravity wave. For all model, there is clear dipole of geopotential signal aligned on the equator, and the regions of horizontal convergence and rainfall, which is about equally contributed by zonal and meridional convergence, exist to the west of the positive geopotential anomaly. In AGUforAPE and LASG, the rainfall represents wavy variation. It should be mentioned that the low level convergence is preceding the precipitation maximum by about 5 degrees. The structure in the upper troposphere (Fig. 17) is, unlike for the composite of Kelvin wave component, similar to that of that of shallow water westward propagating equatorial gravity wave. The signature of the each variable is contrary to that of the corresponding variable in the low level except that whole of the structure is shifted to the east; the area of the horizontal divergence is located to the east of the precipitation maxima by $5 - 10$ degrees, being consistent with the eastward tilt of the vertical velocity anomaly shown later. The smaller degree of the model dependence of the upper tropospheric horizontal structure of the gravity wave component compared to that of the Kelvin wave component can be understood if we keep the direction of the two disturbance components in mind; the gravity wave component propagates westward so that Doppler shifted phase velocity in the troposphere is not small in anywhere in the troposphere, but it becomes small in the upper troposphere for the

Kelvin component as mentioned previously.

Fig. 18 shows the vertical structure of temperature superposed on zonal wind and vertical velocity along the equator for the WIG component. Fig. 19 is but for specific humidity. Like for the Kelvin wave component they display a wide variety. Shallow signal at the melting level and near the surface are notable. Other temperature features seems to be more complex than often found first or second baroclinic mode structure. A pair of temperature dipole in the lower troposphere in GSFC, warm to the west and cool to the east of the precipitation maxima, is one of such examples. The intensity of temperature anomaly, vertical velocity, and specific humidity is large in GSFC, LASG, where the activity of WIG is significant. Vertical velocity signal has some eastward tilt in many of the models, being in consistent with wave-CISK theory. The west-moist east-dry signal in the lower troposphere in CSIRO, EC05, EC07 are more evident those for the Kelvin component (Fig. 12) zonally reversed. In GSFC, as for K, the humidity signal tilts backward. In GSFC and NCAR, east-west contrast of humidity near the surface is notable. In EC05, where strong WIG activity exists, the intensity of the disturbance seems to be rather weak. However, as noted earlier, the plotted quantities are the coefficients of regression to the unit amount of precipitation, so that, in EC05 that has quite large amplitude of WIG component of precipitation, the amplitude of WIG component actually emerging in the model is quite significant.

The composite structure of temperature tendencies due to parameterized convection, DTCONV, and that due to resolved clouds, DTCLD, on the equator are shown in Fig. 20 and Fig. 21, respectively. The structure of DTCONV in each model is generally similar to that in the composite of Kelvin component in the corresponding model. If we compare carefully, however, the vertical distribution of the heating is shifted a bit to the lower altitudes than for the Kelvin filtered component in all models. The structure of DTCLD is also generally similar to that in the composite of Kelvin component in the corresponding model, except that the zonal direction is reversed and the zonal extent is shortened to about one-third. The structure of DTCLD for WIG in NCAR seems to be considerably different from that for K. However, considering more solitary distribution of rainfall in WIG composite and more wavy one in K composite, the structure for WIG should be more directly represent the DTCLD associated with a single rainfall event. Indeed, the west-moist east-dry structure in WIG can easily understood as representation of shallow cloud activity preceding the updraft and the evaporation of stratiform-type rainfall.

In summary, the composite structure of WIG filtered component has a character of the westward propagating inertio gravity waves. In parallel with Kelvin component, the vertical structure of composite disturbances, having tilted updrafts and temperature field in some models, is similar to the unstable mode of wave–CISK. The same caution on the applicability of the classical wave-CISK theory also applies to WIG filtered composite disturbance. In particular, the WIG disturbance in GSFC, being associated with cold downward motion region in the lower troposphere that should generate kinetic energy, is considerable deviation from the simple wave-CISK that primarily focus on the effect of (positive) condensation in convective clouds.

c. Advective component

Fig. 22 shows the horizontal structure of precipitation and horizontal wind on 925hPa for the AD filtered composite. In all models, the precipitation anomaly is confined both meridionally and longitudinally. The zonal extent is much smaller than those for K or WIG components, There is negative anomaly to the east and west of the main positive anomaly in EC05 and LASG. In NCAR, there are two area of negative anomaly in off-equator. The horizontal wind anomaly differ among the models as is in those on 850hPa surface shown below. Fig. 23 shows the horizontal structure of geopotential and horizontal wind on 850hPa surface for the advective component. Reflecting the significant diversity fond in the lower level structure in various models described above, the horizontal structure

Fig. 22
Fig. 23
Fig. 24
Fig. 25
Fig. 26
Fig. 27
Fig. 28

of low level signal is also strongly model dependent. In AGUforAPE, there is a pair of cyclone straddling the equator at the location of maximum precipitation. More or less similar pair of cyclones can be noted also in CSIRO, but they are located nearer to the equator. In ECMWF05, there is a low pressure anomaly on the equator at the maxima of precipitation, but, in contrast to the vorticity dominated flow in AGUforAPE, the low level flow converges directly without appreciable curvature. In ECMWF07, the low level signal is weak and anticyclonic. In GSFC, the maxima of precipitation accompanies distinct high pressure anomaly and divergence, and the flow to the east exhibits anticyclonic circulation. In LASG, a low pressure area on the equator is located at the precipitation maxima, and convergent flow is observed just to the west. The signal is weak in NCAR. In contrast to the diversity in the low level described above, the signal in the upper troposphere (Fig. 24) in all of the model are similar to each other, being characterized with a compact high pressure anomaly from which horizontal wind diverges almost isotropically.

Fig. 25 shows the vertical structure of temperature, zonal wind, and vertical velocity along the equator for the advective component. Fig. 26 shows but for humidity anomaly. The structure of the signal is extremely model dependent. ECMWF05 is characterized with a deep warm core through which an upright ascending motion exists. AGUforAPE is unique in the presence of a intense low level warm anomaly. These two are common in lacking the cool anomaly near the surface that are seen in most of the other models; a lower tropospheric warm core exists also in CSIRO, but it exhibits a distinct surface cold signal. ECMWF07, GSFC, and NCAR are common in that lower troposphere below the melting level $\sim$ 600hPa is cool, and EC07 has a distinct cool region near the surface. Characteristics of lower tropospheric vertical velocity varies even in the three models; updraft dominates in EC07, but it is almost absent in NCAR, and further, downward motion dominates in GSFC. LASG exhibits a cold anomaly in the low level, a warm anomaly around 500hPa, and a cold anomaly near the tropopause; shallow cold anomaly that is found in other models, presumably associated with the parameterized melting of icy hydrometeors, is absent. Humidity structure is characterized with zonally confined positive anomaly at the location of precipitation, but its vertical structure is model dependent. In AGUforAPE and LASG, the updraft is wholly covered by deep moist anomaly. Middle to upper troposphere is moist at the precipitation anomaly also in other models, but lower tropospheric humidity structure is model dependent.

The composite structure of temperature tendencies due to parameterized convection, DTCONV, and that due to resolved clouds, DTCLD, on the equator are shown in Fig. 27 and Fig. 28, respectively. The structure of DTCONV in each model is generally similar to that in the composite of K or WIG component in the corresponding model. If we compare carefully, however, the vertical distribution of the heating is shifted a bit to the higher altitudes than for the K or WIG filtered component in all models. This difference is most notable in NCAR and GSFC. In most models, DTCLD is zonally localized in contrast with the zonally extended distribution realized in K and WIG filtered composite (Fig. 14 for K and Fig. 21 for WIG). GSFC is an exception in that weak sign-reversed component is distributed to the east of the precipitation area. As in K and WIG, the vertical structure of DTCLW are similar to that of DTCONV in AGUforAPE and EC05. In other three models, EC07, GSFC, and, NCAR, lower troposphere is the region of cooling. These cooling, which results presumably from the evaporation of stratiform cooling, nearly cancels the heating due to convection (DTCONV) in these models. The cancellation is consistent with the weak updraft in the lower troposphere in these models.

In spite of the widely different structure among the models described above, we can point out two common features shared in all models; the vertical motions are upright, and are localized around the precipitation maxima. These two points are in contrast with the structure of composite signals found for the Kelvin and gravity wave filtered data, both of which have significant tilting and broader zonal extent. The upright structure of the advective component suggest that it is not wave-CISK but CIFK (conditional instability of the first kind) that drives AD component.

6. Discussions

6.1 Possible mechanism supporting each type of of disturbances

We try to point out possible mechanism that governs the intensity of each filtered component in different models.

a. Kelvin mode

In models with intense Kelvin disturbance, i.e., EC05, EC07 and LASG, (Fig. 4(g)and(l)) the vertical structure of the composite disturbance (Fig. 11(d)and(f)) are similar to the (eastward propagating) unstable modes of wave-CISK (e.g., Hayashi, (1970); Lau and Peng, (1987); Chang and Lim, (1988)) and the observed convectively coupled Kelvin wave (Wheeler and Kiladis 1999); both temperature perturbation and vertical velocity are tilted westward, and the two variables are positively correlated in the upper troposphere, which accounts the conversion from available potential energy to kinetic energy. It may also be noted that the appearance of Kelvin mode commonly appears irrespective of the diversity of upper level structure (Fig. 10). This may suggests that the process in the lower level, where the horizontal structure is farely common in all models (Fig. 8 and Fig. 9).)., is crucial to the excitation of disturbance, not in contradiction to wave-CISK framework in a loose sense stressing the importance of the coupling between convective activity and low level upward motion. It should be stressed that, as was mentioned earlier, vertical structure of heating in each model is confirmed to evolve following the wave phase mainly due to the contribution from (parameterized) stratiform cloud process (Fig. 14); wave-CISK in its original form is not valid in such cases.

In other models, updraft and/or temperature anomaly lacks proper vertical tilt. In CSIRO, updraft is slightly tilted westward, but temperature anomaly is not tilted, and it is tilted eastward in GSFC. In AGUforAPE, only the second baroclinic mode is significant in the temperature anomaly, and the negative correlation of upward motion and temperature in the lower troposphere is unfavorable for the generation of kinetic energy. NCAR seems to be an exception; the temperature anomaly has insignificant tilt (Fig. 11(g)) in spite that Kelvin component is fairly dominant in the relative disturbance intensity (Fig. 6(b)). This strange behavior could be related to its possible connection with n=1 EIG mentioned in Section 4 and/or the off-equatorial structure, both of which await further study.

In order to explain the fact that eastward propagating signal emerge, albeit weak, in CSIRO, GSFC, AGUforAPE, and NCAR, mechanism(s) other than classical wave-CISK may be required. One possibility is the wind-induced surface heat exchange (Emanuel 1987). Another is the forcing from, or the interaction with midlatitude. Supplementary analysis of the model variables in Kelvin component filtered data shows that non negligible correlation exists between the midlatitude meridional wind and the low latitude precipitation in these models, which may support the relationship between the two latitudinal bands. Some authors, for example, Zappa et al (2011) and Straus and Lindzen (2000), suggest the possibility of such interaction, The confirmation of such mechanism in APE data is left for future research.

b. Gravity wave component

Compared to the case of the Kelvin wave diturbances above, the relationship between the structure of disturbance and the intensity of the disturbance in different models is less clear. In the absolute intensity, the gravity wave signal is most intense in ECMWF05 and LASG (Fig. 4(f)and(l)). In these models, temperature disturbance has eastward phase tilt, which is a feature common to an (westward propagating) unstable mode of wave-CISK. Similar tilted structure can be noted for NCAR and ECMWF07 (Fig. 18(d) and (g)), where gravity wave disturbance is not strong. Somewhat stronger warm first baroclinic mode signal may be a factor enhancing wave-CISK in ECMWF05. Measured by the intensity of gravity wave component relative to the total variance (Fig. 6(b)), LASG and GSFC are the models with relatively intense gravity wave component. A common features notable in the gravity wave structure in these two models are strong temperature and vertical velocity perturbations in the lower troposphere (Fig. 18(e) and (f)),. This combination may be preferable to activate the coupling between the gravity wave and convective activity. In GSFC, downward flow in the cool anomaly in the lower troposphere to the east of the precipitation anomaly, which contributes to the release of available potential energy, may be helping the appearance of relatively significant gravity wave component. This cool downdraft is presumably induced by the cooling due to the (parameterized) evaporation of stratiform rain (Fig. 21). Its timescale (1day) and horizontal extent (1000km) are not very different from those of observed mesoscale precipitation systems (Houze and Betts 1981) and WIG (Takayabu 1994b), or so-called "2-day waves" (Haertel and Kiladis 2004), although whether such seemingly superficial correspondence supports particular parameterization of cloud process or not is unclear.

c. Advective component

Advective component is significant in ECMWF05, LASG, and AGUforAPE, measured either by absolute intensity or by its contribution to total precipitation variance (Fig. 6(a) and 6(b)). Before examining factors that make the “advecitve” components in these three models intense, it is important to examine whether the “AD” components in these models should be identified as advective component in more strict sense, whose phase velocity is close to the low level zonal wind near the equator (Wheeler and Kiladis 1999). In the frequency wavenumber spectra (Fig. 4 or 5), we can easily find the AD components in AGUforAPE and LASG have their dominant phase velocity, while we can not for ECMWF05; the AD component spectrum of ECMWF05 is scattered in a wide range with “red” frequency distribution in wavenumber-frequency space. Because of this wide bandwidth, significant portion of power does fall within the defined spectral region of the AD component also in EC05, but it is simply spreading broadly, so that no characteristic velocity can be pointed out. In AGUforAPE and LASG, the dominant westward phase velocity is about 10.3m/s and 7.7 m/s, respectively, which is reasonably close to the zonal mean zonal wind at 850hPa in the corresponding model, which is 11.2 m/s and 8.3 m/s, respectively; Hovmëllor plot for LASG (Fig. 3(l)) may display an impression with much faster phase velocity, but it results from the superposition with faster propagating westward inertio gravity mode. The coincidence of the zonal wind velocity and the phase speed of AD mode suggests that the motion of AD mode is indeed governed by advection of certain physical variables in LASG and AGUforAPE; they are surely “advective” component. On the other hand, EC05 requres more careful examination. In the Hovmëllor plot of precipitation (Fig. 3(f)), we notice that typical grid-scale convection in ECMWF05 is not short-lived; they sometimes last for as long as about 5days. Looking into such cases closely, we can find that the grid-scale convection moves only very slowly; in some cases it does not move at all throughout the 5 day lifetime. This slow movement is not trivial because it can hardly be explained by advection of physical variables by the zonal mean zonal wind, which is -7.5 m/s at 850hpa. More careful examination, however, assures us that they are indeed "advective" feature. Because the location of strong grid-scale convections are, in EC05, typically to the west of the zonal convergent area of the Kelvin wave, so that the westerly wind anomaly at those locations almost completely offsets the zonal mean easterly.

Another issue to be examined is what the physical quantity that keeps the identity of AD component is (are). In AGUforAPE, it seems to be the water vapor mixing ratio, which exhibits a deep positive anomaly at the maxima of precipitation (Fig. 26(a)). The low level vorticity anomaly at the off equatorial portion of the precipitation anomaly (Fig. 23(a)) may contribute to keep the identity of AD component disturbance to some extent. At the same time, the absence of surface cold anomaly, which is one of the unique characters of the composite structure of AD component in

AGUforAPE, is favorable to the longevity of convective activity observed in the Hovmëllor plot (Fig. 3(a)). In LASG positive moisture anomaly at the rainfall maxima is also found (Fig. 26(f)), but we are less confident on the feasibility of the moisture anomaly as the mechanism serving as the memory variables to be advected, because the low level cold anomaly (Fig. 25) may prevent persistent convective activity as is discussed below.

If we compare the composite vertical structures in the models with significant AD components, namely ECMWF05 and AGUforAPE, with those in the models with weaker AD components (Fig. 25 and 26), we comes to the idea that cold anomaly in the lower troposphere, whether thick (NCAR, ECMWF07, GSFC) or shallow (GSIRO), suppresses the development of the AD component. In other words, we can observe that the AD component or grid scale precipitation is strong and long-lasting when the composite structure of AD component exhibits warm lower troposphere. One extreme case is AGUforAPE, where the full depth of lower troposphere is warm and moist (Fig. 25(a) and 26(a)), Possible factor that contributes to the establishment of the warm core is ineffective evaporation of raindrops in these two models as are suggested in the composite temerature dendency (Fig. 27(a,b) and 28(a,b)).

The absence of rain evaporation is favorable not only for the development of "grid scale convection" by CIFK but also for the maintainance of such disturbance (Nakajima and Matsuno 1988). The other extreme is GSFC, where the evaporation of rain in the lower troposphere seems to be very strong. As shown in Fig. 4(j), AD component is very weak whereas gravity mode is significant instead. The existence of the deep moist core found in AGUforAPE and ECMWF05 (Fig. 26(a)and(c), respectively) may look inconsistent with the ineffective rain evaporation, but one should recognize that the evaporation of rain cools the atmosphere and induce downward motion, which contributes to drying of the atmosphere. Such significant sensitivity of the behavior of grid scale convection to the rain evaporation is demonstrated by the contrast between the behavior of AD components in ECMWF05 and ECMWF07; from the former to the latter, parameterization of rain evaporation are revised so as to increase the efficiency of rain evaporation (Bechtold et al. 2008). It is interesting to note that, the revision results in the enhancement of Kelvin wave signal, although the reason remain unclear.

6.2 Comparison with observed Convectively Coupled Equatorial Waves

It would be useful to compare the behavior of the CCEWs simulated in APE runs with those in the real atmosphere. However, we should be cautious in such comparison for at least two reasons. First, behavior of atmospheric disturbances depends on the surface boundary conditions, where the APE and the real atmosphere differ consideably: the SST in the real atmosphere is not zonally symmetric at all, whereas no land surface is assumed in the experiments in the APE. Second, quantities observed in the real atmosphere do not necessarily have temporal and/or spatial coverage, resolution, and uniformity. The attempts of such comparison which follows, therefore, inevitably remain superficial.

The wavenumber frequency spectra of OLR in the equatorial area has been has been examined by a number of authors including Takayabu (1994a), Wheeler and Kiladis (1999). Cho et al (2004) examine the precipitation data from TRMM, and show that the type and character of CCEWs found in the precipitation data is consistent with those in OLR data. In the annual average of equatorially symmetric component, shown in Fig.3(b) of WK99, that Kelvin and the equatorial Rossby signals are strong, and that weaker but significant westward inertio gravity mode, whose dominant wavenumber is larger than 4, and "TD-type" signal exist. WK99 also examines the seasonal variation of the spectra. Their Fig.5(b)and(d) show significantly different character of wave activity. TD-type signal is much stronger in northern summer, whereas other types are stronger in southern summer. The dominant wavenumber of the westward inertio gravity mode signal varies seasonally, which is 2–7 in souther summer and is larger than 7 in northern summer. Considering that the meridional distribution of SST prescribed in the experiments analyzed in this paper is more similar to that of southern summer rather than to that of northern summer, we would expect weak AD component and strong K and WIG components. As was described in Section 4, most model are, to some extent successful in reproducing K component. Abundant presence of AD component in APE models might be aganst the expectation above. However, the latitudinal distribution of AD component in APE may differ from the "TD-type" signal in WK99; with the sharp peak of SST in APE CONTROL (Fig. 1), convective activity in the off-equatorial latitudes, which is one of the necessary ingredient of "TD" in the real atmosphere, can not occur actively, and the AD component disturbance analyzed in this study may be different from the "TD-type" signal in WK99. Instead, the AD component in this study may be related to "background" component in WK99. In APE, WIG signal appears clearly only in a limited models; among the seven models that are intensively analyzed, EC05, LASG, and GSFC represent appreciable WIG signal, and, NICAM and K1JAPAN among the models not analyzed deeply. However, EC05 seems to be unsuccessful in presenting the WIG as a dominant signal along dispersion curves of equatorial WIG mode. GSFC does not suceed in the representation of long wavelength WIG component.

The spatial structure of CCEWs have been subject to a number of research, such as Wheeler et al (2000), Yang et al (2007a,2007b,2007c) and other studies reviewed by Kiladis et al (2009). It has been established that Kelvin mode and westward inertio gravity mode have "boomerang" like structure temperature anomaly, which can be interpreted as the internal wave emitted upward and downward from the strong convective heating at the updraft phase to the direction of propagation (Fig.7 in WK99 for Kelvin mode, and Fig.23 for WIG mode). The contrast of humidity in the lower troposphere, more humid before the convection and drier after, is another important feature. Such structure is reproduced in only a small number of models in APE analyzed here: EC05, EC07 and LASG are good in performance in Kelvin component, and only LASG is good for WIG component. The performance of NICAM in representation of Kelvin like structure, as is extensively described in Nasuno et al (2008), seems to be quite successful, but that for WIG is not known.

Horizontal structures of Kelvin and Rossby modes in the real atmosphere are extracted and investigated by Yang et al (2007c), where the analysis are conducted bearing the difference between the structures of waves on the eastern and western hemispheres in mind. Comparing with Kelvin mode structure in Fig.1 of Yang et al (2007c), we can find that the Kelvin mode in the APE examined here is more similar to that in the western hemisphere, noting the presence of significant meritional wind perturbation in the lower troposphere and considerable rotational wind component in the upper troposphere. Either of the structures of Rossby mode presented in Fig.5 for the western hemisphere and Fig.9 for the eastern hemisphere of Yang et al (2007c) is not similar to that of advective component in most of the APE models presented here, in that those observed Rossby modes contains a pair of distinct off-equatorial vortical cells in the lower troposphere. As is noted earlier, such off-equatorlai low level rotational signal can be noted only in a small number of models (AGUforAPE and CSIRO); even in these models, the location of the maximum of vorticity is much nearer to the equator compared with the those in Yang et al (2007c). The composite structure of Kelvin and Rossby modes presented in Kiladis et al (2009) exhibit features common to those in Yang et al (2007c). Finally, the horizontal structure of WIG presented in Kiladis et al (2009) is generally in good agreement with WIG in the present APE results.

The difference between the properties of their Rossby modes and the present advective components may be quite natural considering the difference between the definition of the Rossby modes in those papers and that of the "advective" component in this paper. Direct comparison requires additional analysis focusing more sharply on the Rossby modes, which is left for a future study. Another factors that may contribute to the difference in all types of disturbances is the difference of meridional structure of SSTs in the real atmosphere and the CONTROL profile of APE. In this respect, it would be useful to compare the structure of convectively coupled equatorial waves tha appear in the APE experiments with the SST profiles other than CONTROL, but it is left for future study, because complete re-run of the models are indispensable in order to collect the necessary data.

It is interesting to note that, together with NICAM, which is with no doubt one of the most advanced models, and LASG, which is equipped with the simplest convective adjustment (Manabe et al. 1965), outperform most other models with various kind of more complex cumulus schemes in several aspects incuding the reproduction of the spectrum of WIG and the structure of CCEWs. Of course, at least the former of the two may not be surprizing because most AGCMs are tuned to reproduce climatological states of the atmosphere, so that WIG, which isshort period and their relationship to the long-time and/or large-scale atmospheric variables is unclear, has not been subject to extensive tuning. The situation might has changed a lot since the execution of APE, and more recent generation of models may perform much better.

6.3 Comparison with Convectively Coupled Equatorial Waves represented in previous modeling studies

Convectively coupled Kelvin mode has been investigated in several modeling studies including those with the aqua planet setup (e.g., Frierson, 2007; Lee et al, 2003) or those with realistic surface boundary condition (e.g., Lee et al, 2003; Suzuki et al,2006; Frierson et al, 2010). These studies are aimed at improvement of the representation of Kelvin modes with more or less amount of "tuning" of the model. The structure of Kelvin modes simulated in those studies, with successful performance in particular, shares several aspects with observed waves such as the "boomerang" like structure temperature. Compared with the similarity among those "successful" cases, the structure of the Kelvin mode in APE experiments described in this paper exhibits by far wider variety. Somewhat similar intercomparison is done on Kelvin waves in CMIP3 (Coupled Model Intercomparison Project phase 3) by Straub et al (2010). Although the comparison of the structure is, as in the present paper, limitted to a small number of models, considerable diversity is found both in horizontal and in vertical structure, again as in the present paper. All of these past and present results suggest that there is much room for improvement of the representation of Kelvin modes.

Rossby mode, possibly corresponding to the advective component in the present paper to some degree, and WIG mode have not investigated so intensively with general circulation models. Suzuki et al (2006) examines Rossby modes focusing on the sensitivity to a modification of cumulus parameterization. The horizontal structure of Rossby modes in their experiments resembles no to those in the APE described in this paper but to that of the observed waves (Kiladis et al. 2009), again suggesting the possible importance of the choice of the SST profile noted earlier.

6.4 Other branches in the frequency wavenumber space

With different specification of SST profile, the space time structure of the equatorial precipitation varies as is described in Blackburn et al (2011b). Still, most of the features in the space time spectra can be classified as Kelvin, advective and WIG signals as are described above. However, relative power among the three types of signals varies reflecting the change of space time structure of precipitation responding to the change of SST profile. Here we mention only two of the notable features in experiment with the SST profile other than CONTROL.

In FLAT experiment of ECMWF-07, not only n=1 WIG but also n=1 EIG signal can be distinctly appears. This may be understandable considering that the width of equatorial precipitation region is much broader with the FLAT SST profile than with the CONTROL SST, so that the EIG , which have more latitudinally extended region of convergence than

WIG, can interact with moist convection more easily. Actually, the power of the EIG is found in the symmetric component of the precipitation in the latitude band of 10-20 degree (not shown), which corresponds to the off-equatorial peak of convergence in n=1 EIG, for example, see Fig.3 of Yang et al (2003). However, the reason why n=1 EIG does not appear in other FLAT experiment with models other than ECMWF-07 in spite that most of them are characterized with equally broad ITCZ.

We mentioned the possible existence of the eastward propagating inertio gravity waves also in CNTL of NCAR. We did not perform detailed analysis on the off equatorial structure, so that no firm conclusion is admitted presently. It may worth noted, however, that the appearance of the eastward gravity wave mode in CNTL of NCAR is consistent with that in FLAT of ECMWF07; they are cases with double ITCZ or broad ITCZ, which allows the coupling between the convective heating and the wave motion not only at the equator but also that in off-equatorial latitude. Still, the coupling may not be simple, because, in spite that ITCZ is broad or double in some experiments other than CTCL of NCAR and FLAT of ECMWF07, eastward inertio gravity wave signal can not be identified in those models. To solve these issues, further investigation is necessary with more augmented datasets provided by re-run of models.

6.5 Relationship between the height of convective heating and phase speed of disturbance

In all models, the vertical structure of convective heating in the three spectral filtered composite are slightly different (Fig. 13, Fig. 20,Fig. 27). If we compare them carefully, we can notice that, in each model, the "center of gravity" of the convective heating is located at lowest level in WIG, a little higher level in K, and at heighest level in AD. Interestingly, the above order follows the reverse of the phase velocity of the three components relative to the low level zonal wind. In other words, if this is true, the faster the intrinsic phase velocity of the disturbance, at the lower level the convective heating occurs. Such tendency might be natural if one recalls that the development of (parameterized) moist convection requires certain degree of moisture accumulation, for which certain length of time would be necessary; if the wave period be shorter than the moisture accumulation time scale, the convective heating might be unable to respond. This sensitivity of the heating to the period of disturbance is similar to, but slightly different from, the idea of "phase lagged wave-CISK" proposed by Davies (1979), or the effect of "convective response time" discussed by several authors (e.g. Emanuel,1993; Emanuel et al, 1994; Lindzen, 2003). In phase-lagged wave-CISK, phase between the heating and the low level upward motion is assumed to depend on the wave period, and in the formulation in Emanuel(1993), the intensity of the heating is assumed to depend on the wave period, whereas in the present analysis, the vertical structure of the heating is shown to depends on the wave period. This is an interesting possibility which could lead to another way of eliminating the "ultraviolet catastrophe" from classical wave-CISK. However, before going further, how such dependency emerge in the models should be investigated especially because such intricate character on the interaction between convection and large-scale motion is expected to be an difficult issue in the performance of cumulus parameterization in general. This issue is left for future research.

7. Concluding remarks

We have examined the results of the Aqua Planet Experiment project focusing mainly on the structure of equatorial precipitation in the subset of participating models on which details of model variables are available. The summary of results are presented in abstract so is not repeated here.

We can say that the simple and idealized setup of the APE project has been quite successful in elucidating the similarity and difference of the equatorial precipitation structure in different models. However, it is still difficult to explain what kind of differences in the choice of parameterizations of physical processes are related to particular differences of the composite structure. The source of difficulty is at least three-fold. First, the different cumulus parameterizations contain different sets of internal variables and the output variables, so that meaningful comparison among the behavior of parameterizations is a difficult task. Second, partly due to the difficulty noted above, we could not define appropriate datasets to describe the behavior of parameterizations of physical processes in advance, so that could not obtain consistent datasets from the participating groups. Third, as is almost always applies to the analysis of the atmospheric models, complex entangled interplay among various dynamical and physical processes in the models makes clear, simple interpretation impossible in spite of the simple and unified external setup of Aqua Planet Experiments.

We can not be sure on to what extent the results of the present study applies to the behavior of precipitation features in more realistic setup. This is partly because we analyze only subset of CTRL experiments, which is, in itself, a subset of the specifications in APE project. It should be bear in mind that the CTRL case may not be most "realistic" setup among the cases defined in APE project. For example, as described in Blackburn et al (2011a), Ohfuchi et al (2011) and the APE-ATLAS (Williamson et al. 2011), the tropospheric jets in CTRL case are too strong and located at lower latitude compared to the climatological zonal mean state of the real atmosphere, and the ITCZ precipitation is, in most models, too much concentrated at the equator. The former point may affect the intensity and character of the interaction between the tropics and mid-latitudes, and the latter point may affect on many aspects of properties of convectively coupled equatorial disturbances, i.e., the main results of this study. It is clear that the present analysis should be supplemented by the analysis of other cases, i.e., FLAT, QOBS and PEAKED cases. However, regrettably, the composite analysis of those cases requires time series of three dimensional model variables and tendency data that were not submitted on the most of the participating models.

Lastly, we comment on the necessity of "APE2", i.e., another execution of aqua planet experiment project. The numerical experiments for the present APE by the participating groups were conducted in the period of 2002–2007. Some of the results of this study, namely the large degree of diversity found in the properties of precipitation such as the intensity of Kelvin, gravity, and advective components and the vertical structure of the composite structure of the three, may originate from immaturity of the atmospheric models in that period. The same can be said about other diversity found among the different models described in APE-ATLAS and Blackburn et al (2011ab). Because global atmospheric models have been developing extensively in many aspects such as spatial resolution and the parameterizations, it is worth repeating the Aqua Planet Experiment project in a basically the same framework. It is particularly interesting to examine whether the current generation of atmospheric models will still exhibit diversity like shown in this paper or not. In the possible repetition of APE, it should be important to collect more complete datasets on all of the cases; the time series of low level atmosphere would be indispensable to examine the tropical disturbances. Finally, it should be stressed that, not only to compare but also to interpret the results of experiments, complete enough description of numerical models is indispensable. It would be ideal that every participating group would provide the source code of the numerical model used and interested members can re-run models of other groups. Such deep collaboration may not be so easy, but would be very fruitful to advancement of modeling community.

Acknowledgements

The authors thank the APE participants of CSIRO, ECMWF, GSFC, LASG, and, NCAR for providing the additional transient data used in this study. Numerical integration of AGU model were performed at the Earth Simulator Center. Analysis software and local computational environments were constructed by the use of the resources of GFD-DENNOU-CLUB (http://www.gfd-dennou.org), including GPhys (http://ruby.gfd-dennou.org), spmodel (http://www.gfd-dennou.org/library/spmodel), and DCL (http://www.gfd-dennou.org/library/dcl). This work was supported by Grants-in-Aid(B) for

Scientific Research (12440123 and 21340139).

References

Arakawa, A., and W. Schubert, 1974: Interaction of a cumulus cloud ensemble with the large-scale environment, part i. *J. Atmos. Sci*, **31(3)**, 674–701.

Bechtold, P., M. Köhler, T. Jung, F. Doblas-Reyes, M. Leutbecher, M. Rodwell, F. Vitart, and G. Balsamo, 2008: Advances in simulating atmospheric variability with the ecmwf model: From synoptic to decadal time-scales. *Quarterly Journal of the Royal Meteorological Society*, **134(634)**, 1337–1351.

Blackburn, M., and B. Hoskions, 2011: Context and aims of the aqua planet experiment. *J. Meteor. Soc. Japan*, **??**, submitted.

Blackburn, M., D. L. Williamson, K. Nakajima, W. Ohfuchi, Y. O. Takahashi, Y.-Y. Hayash, H. Nakamura, M. Ishiwatari, J. McGregor, H. Borth, V. Wirth, H. Frank, P. Bechtold, N. P. Wedi, H. Tomita, M. Satoh, M. Zhao, I. M. Held, M. J. Suarez, M.-I. Lee, M. Watanabe, M. Kimoto, Y. Liu, Z. Wang, A. Molod, K. Rajendran, K. A., and R. Stratton, 2011a: The aqua planet experiment (ape): Control sst simulation. *J. Meteor. Soc. Japan*, **??**, submitted.

Blackburn, M., D. L. Williamson, K. Nakajima, W. Ohfuchi, Y. O. Takahashi, Y.-Y. Hayash, H. Nakamura, M. Ishiwatari, J. McGregor, H. Borth, V. Wirth, H. Frank, P. Bechtold, N. P. Wedi, H. Tomita, M. Satoh, M. Zhao, I. M. Held, M. J. Suarez, M.-I. Lee, M. Watanabe, M. Kimoto, Y. Liu, Z. Wang, A. Molod, K. Rajendran, K. A., and R. Stratton, 2011b: The aqua planet experiment (ape): Response to changed meridional sst profile. *J. Meteor. Soc. Japan*, **??**, submitted.

Chang, C., and H. Lim, 1988: Kelvin wave-cisk: A possible mechanism for the 30-50 day oscillations. *Journal of the atmospheric sciences*, **45(11)**, 1709–1720.

Cho, H., K. Bowman, and G. North, 2004: Equatorial waves including the madden-julian oscillation in trmm rainfall and olr data. *Journal of Climate*, **17(22)**, 4387–4406.

Davies, H., 1979: Phase-lagged wave-cisk. *Quarterly Journal of the Royal Meteorological Society*, **105(444)**, 325–353.

Emanuel, K., 1987: An air-sea interaction model of intraseasonal oscillations in the tropics. *Journal of the atmospheric sciences*, **44(16)**, 2324–2340.

Emanuel, K., 1993: The effect of convective response time on wishe modes. *Journal of the atmospheric sciences*, **50(12)**, 1763–1763.

Emanuel, K., J. David Neelin, and C. Bretherton, 1994: On large-scale circulations in convecting atmospheres. *Quarterly Journal of the Royal Meteorological Society*, **120(519)**, 1111–1143.

Frierson, D., 2007: Convectively coupled kelvin waves in an idealized moist general circulation model. *Journal of the atmospheric sciences*, **64**, 2076–2090.

Frierson, D., D. Kim, I.-S. Kang, M.-I. Lee, and J. Lin, 2010: Structure of agcm-simulated convectively coupled kelvin waves and sensitivity to convective parameterization. *Journal of the atmospheric sciences*, **68**, 26–45.

Gill, A., 1982: Studies of moisture effects in simple atmospheric models: The stable case. *Geophysical & Astrophysical Fluid Dynamics*, **19(1-2)**, 119–152.

Haertel, P., and G. Kiladis, 2004: Dynamics of 2-day equatorial waves. *Journal of the atmospheric sciences*, **61(22)**, 2707–2721.

Hayashi, Y., 1970: A theory of large-scale equatorial waves generated by condensation heat and accelerating the zonal wind. *J. Meteor. Soc. Japan*, **48**, 140–160.

Hayashi, Y., and A. Sumi, 1986: The 30-40 day oscillations simulated in an "aqua planet" model. *J. Meteor. Soc. Japan*, **64**, 451–467.

Hendon, H., and M. Wheeler, 2008: Some space-time spectral analyses of tropical convection and planetary-scale waves. *Journal of Atmospheric Sciences*, **65**, 2936.

Houze, Jr, q. R., and A. Betts, 1981: Convection in gate. *Reviews of Geophysics*, **19(4)**, 541–576.

Kiladis, G., M. Wheeler, P. Haertel, K. Straub, and P. Roundy, 2009: Convectively coupled equatorial waves. *Rev. Geophys*, **47**.

Kuang, Z., P. Blossey, and C. Bretherton, 2005: A new approach for 3d cloud-resolving simulations of large-scale atmospheric circulation. *Geophys. Res. Lett*, **32(L02809)**, 1–4.

Lau, K., and L. Peng, 1987: Origin of low-frequency (intraseasonal) oscillations in the tropical atmosphere. part i: Basic theory. *Journal of Atmospheric Sciences*, **44**, 950–972.

LEE, M., I. KANG, and B. MAPES, 2003: Impacts of cumulus convection parameterization on aqua-planet agcm simulations of tropical intraseasonal variability. *Journal of the Meteorological Society of Japan*, **81(5)**, 963–992.

Lindzen, R., 2003: The interaction of waves and convection in the tropics. *Journal of Atmospheric Sciences*, **60**, 3009–3020.

Madden, R., and P. Julian, 1972: Description of global-scale circulation cells in the tropics with a 40–50 day period. *J. Atmos. Sci*, **29(6)**, 1109–1123.

Madden, R., and P. Julian, 1994: Observations of the 40-50-day tropical oscillation-a review. *Monthly Weather Review*, **122(5)**, 814–837.

Manabe, S., J. Smagorinsky, and R. Strickler, 1965: Simulated climatology of a general circulation model with a hydrologic cycle 1. *Monthly Weather Review*, **93(12)**, 769–798.

Mapes, B., S. Tulich, J. Lin, and P. Zuidema, 2006: The mesoscale convection life cycle: Building block or prototype for large-scale tropical waves? *Dynamics of atmospheres and oceans*, **42(1-4)**, 3–29.

Matsuno, T., 1966: Quasi-geostrophic motions in the equatorial area. *J. Meteor. Soc. Japan*, **44(1)**, 25–42.

Matthews, A., and R. Madden, 2000: Observed propagation and structure of the 33-h atmospheric kelvin wave. *Journal of the atmospheric sciences*, **57(21)**, 3488–3497.

Miura, H., H. Tomita, T. Nasuno, S. Iga, M. Satoh, and T. Matsuno, 2005: A climate sensitivity test using a global cloud resolving model under an aqua planet condition. *Geophys. Res. Lett*, **32**, L19717.

Nakajima, K., and T. Matsuno, 1988: Numerical experiments concerning the origin of cloud clusters in the tropical atmosphere. *J. Meteor. Soc. Japan*, **66**, 309–329.

Nasuno, T., H. Tomita, S. Iga, H. Miura, and M. Satoh, 2008: Convectively coupled equatorial waves simulated on an aquaplanet in a global nonhydrostatic experiment. *Journal of the Atmospheric Sciences*, **65(4)**, 1246–1265.

Neale, R., and B. Hoskins, 2000: A standard test for agcms including their physical parametrizations: I: The proposal. *Atmospheric Science Letters*, **1(2)**, 101–107.

Numaguti, A., and Y. Hayashi, 1991a: Behavior of cumulus activity and the structures of circulations in an" aqua planet" model part i: The structure of the super clusters. *J. Meteor. Soc. Japan*, **69**, 541–561.

Numaguti, A., and Y. Hayashi, 1991b: Behavior of cumulus activity and the structures of circulations in an" aqua planet" model part ii: Eastward-moving planetary scale structure and the intertropical convergence zone. *J. Meteor. Soc. Japan*, **69**, 563–579.

Satoh, M., T. Matsuno, H. Tomita, H. Miura, T. Nasuno, and S. Iga, 2008: Nonhydrostatic icosahedral atmospheric model (nicam) for global cloud resolving simulations. *Journal of Computational Physics*, **227(7)**, 3486–3514.

Sherwood, S., R. Roca, T. Weckwerth, and N. Andronova, 2010: Tropospheric water vapor, convection, and climate. *Rev. Geophys*, **48**, RG2001.

Straub, K., P. Haertel, and G. Kiladis, 2010: An analysis of convectively coupled kelvin waves in 20 wcrp cmip3 global coupled climate models. *Journal of Climate*, **23(11)**, 3031–3056.

Straus, D., and R. Lindzen, 2000: Planetary-scale baroclinic instability and the mjo. *Journal of the atmospheric sciences*, **57(21)**, 3609–3626.

Suzuki, T., Y. Takayabu, and S. Emori, 2006: Coupling mechanisms between equatorial waves and cumulus convection in an agcm. *Dynamics of atmospheres and oceans*, **42(1-4)**, 81–106.

Takayabu, Y., 1994a: Large-scale cloud disturbances associated with equatorial waves. i: Spectral features of the cloud disturbances. *Journal Of The Meteorological Society Of Japan*, **72(3)**, 433–449.

Takayabu, Y., 1994b: Large-scale cloud disturbances associated with equatorial waves. ii: Westward-propagating inertio-gravity waves. *Journal of the Meteorological Society of Japan*, **72(3)**, 451–465.

Tao, W., and M. Moncrieff, 2009: Multiscale cloud system modeling. *Reviews of Geophysics*, **47(4)**, RG4002.

Tiedtke, M., 1989: A comprehensive mass flux scheme for cumulus parameterization in large- scale models. *Monthly Weather Review*, **117(8)**, 1779–1800.

Wheeler, M., and G. Kiladis, 1999: Convectively coupled equatorial waves: Analysis of clouds and temperature in the wavenumber-frequency domain. *Journal of Atmospheric Sciences*, **56**, 374–399.

Wheeler, M., G. Kiladis, and P. Webster, 2000: Large-scale dynamical fields associated with convectively coupled equatorial waves. *Journal of the Atmospheric Sciences*, **57(5)**, 613–640.

Williamson, D. L., M. Blackburn, B. Hoskins, K. Nakajima, W. Ohfuchi, Y. O. Takahashi, Y.-Y. Hayash, H. Nakamura, M. Ishiwatari, J. McGregor, H. Borth, V. Wirth, H. Frank, P. Bechtold, N. P. Wedi,

H. Tomita, M. Satoh, M. Zhao, I. M. Held, M. J. Suarez, M.-I. Lee, M. Watanabe, M. Kimoto, Y. Liu, Z. Wang, A. Molod, K. Rajendran, K. A., and R. Stratton, 2011: *The APE Atlas. NCAR/TN-484+STR*. Natilnal Center for Atmospheric Research.

Woolnough, S., J. Slingo, and B. Hoskins, 2004: The diurnal cycle of convection and atmospheric tides in an aquaplanet gcm. *Journal of the atmospheric sciences*, **61(21)**, 2559–2573.

Yang, G., B. Hoskins, and J. Slingo, 2003: Convectively coupled equatorial waves: A new methodology for identifying wave structures in observational data. *Journal of the atmospheric sciences*, **60(14)**, 1637–1654.

Yang, G., B. Hoskins, and J. Slingo, 2007a: Convectively coupled equatorial waves. part i: Horizontal and vertical structures. *Journal of the Atmospheric Sciences*, **64(10)**, 3406–3423.

Yang, G., B. Hoskins, and J. Slingo, 2007b: Convectively coupled equatorial waves. part ii: Propagation characteristics. *Journal of the Atmospheric Sciences*, **64(10)**, 3424–3437.

Yang, G., B. Hoskins, and J. Slingo, 2007c: Convectively coupled equatorial waves. part iii: Synthesis structures and their forcing and evolution. *Journal of the Atmospheric Sciences*, **64(10)**, 3438–3451.

Zappa, G., V. Lucarini, and A. Navarra, 2011: Baroclinic stationary waves in aquaplanet models. *Journal of the atmospheric sciences*, **68(5)**, 1023–1040.

List of Figures

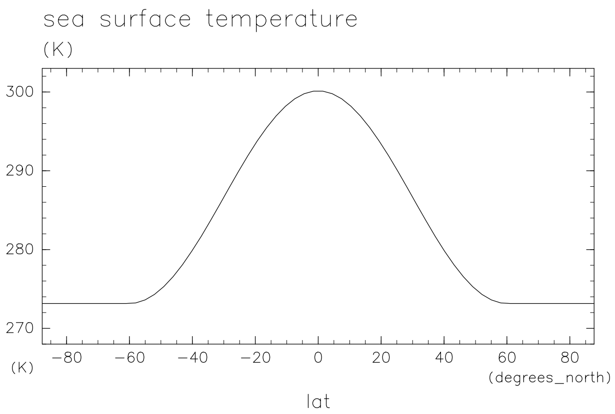

Fig. 1. Meridional distributions of sea surface temperature [K] in CONTROL experiment.

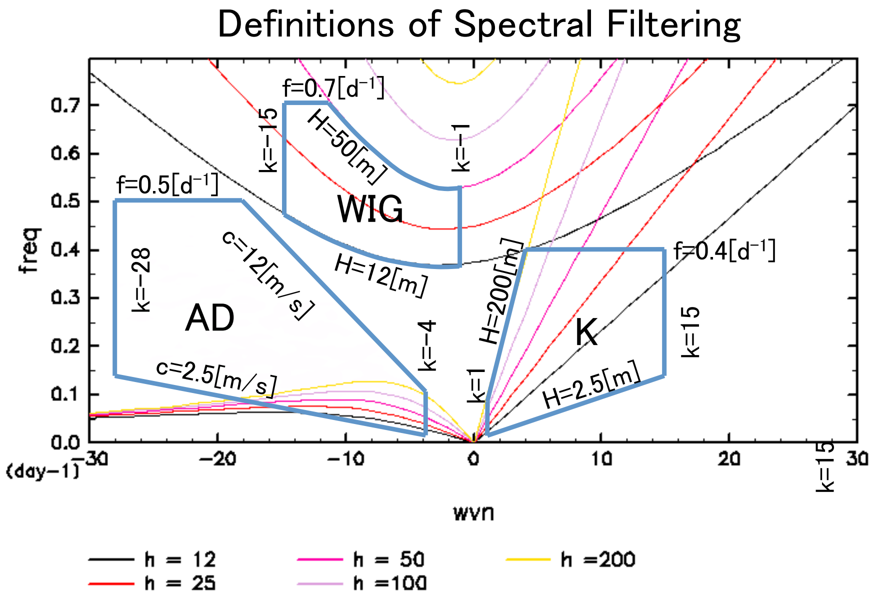

Fig. 2. Definition of spectral filtering.

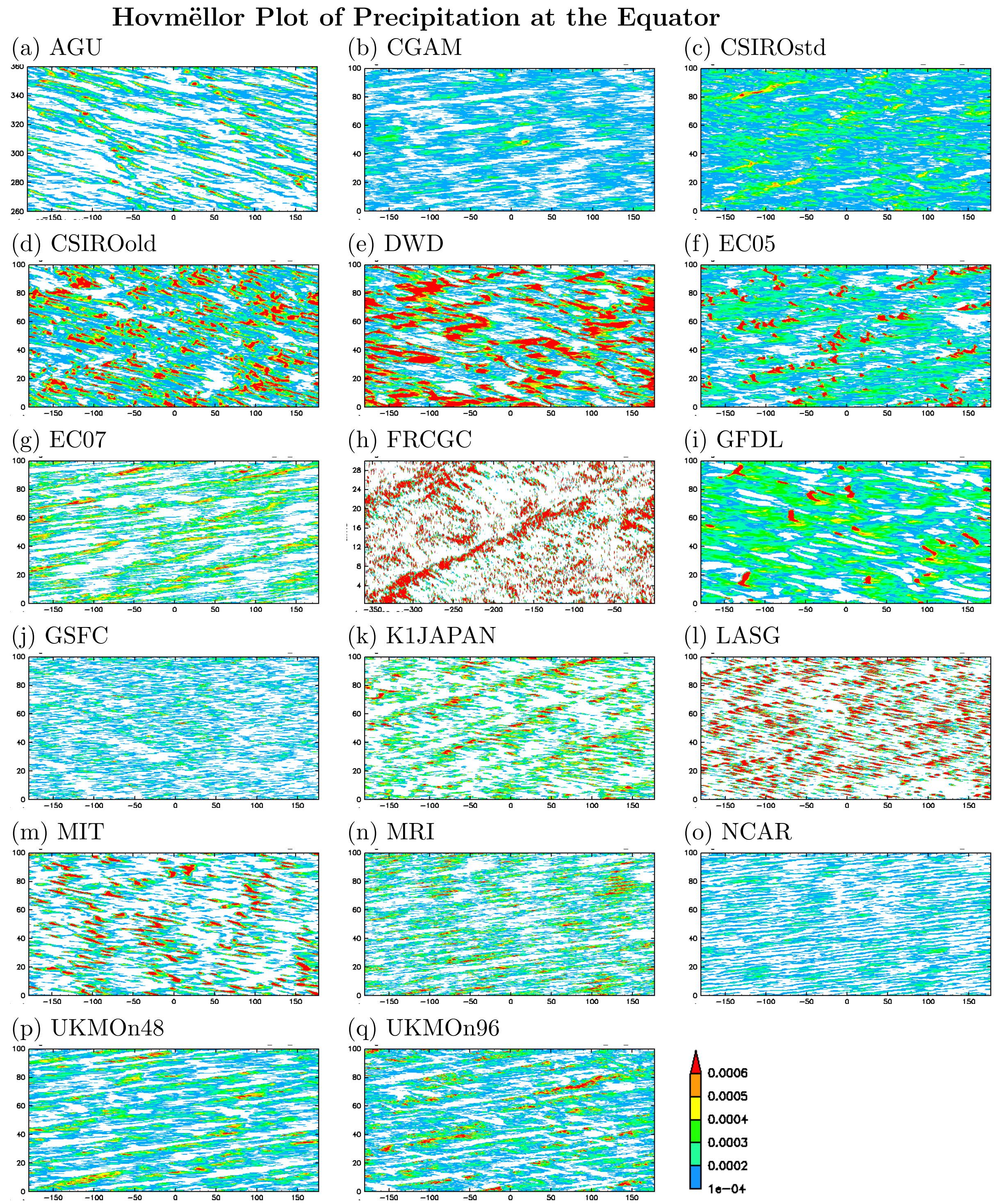

Fig. 3. Hovmëllor plot of equatorial precipitation.The horizontal axis is longitude, and the vertical axis is time going up.Unit is $kg \cdot m^{-2} \cdot s^{-1}$.

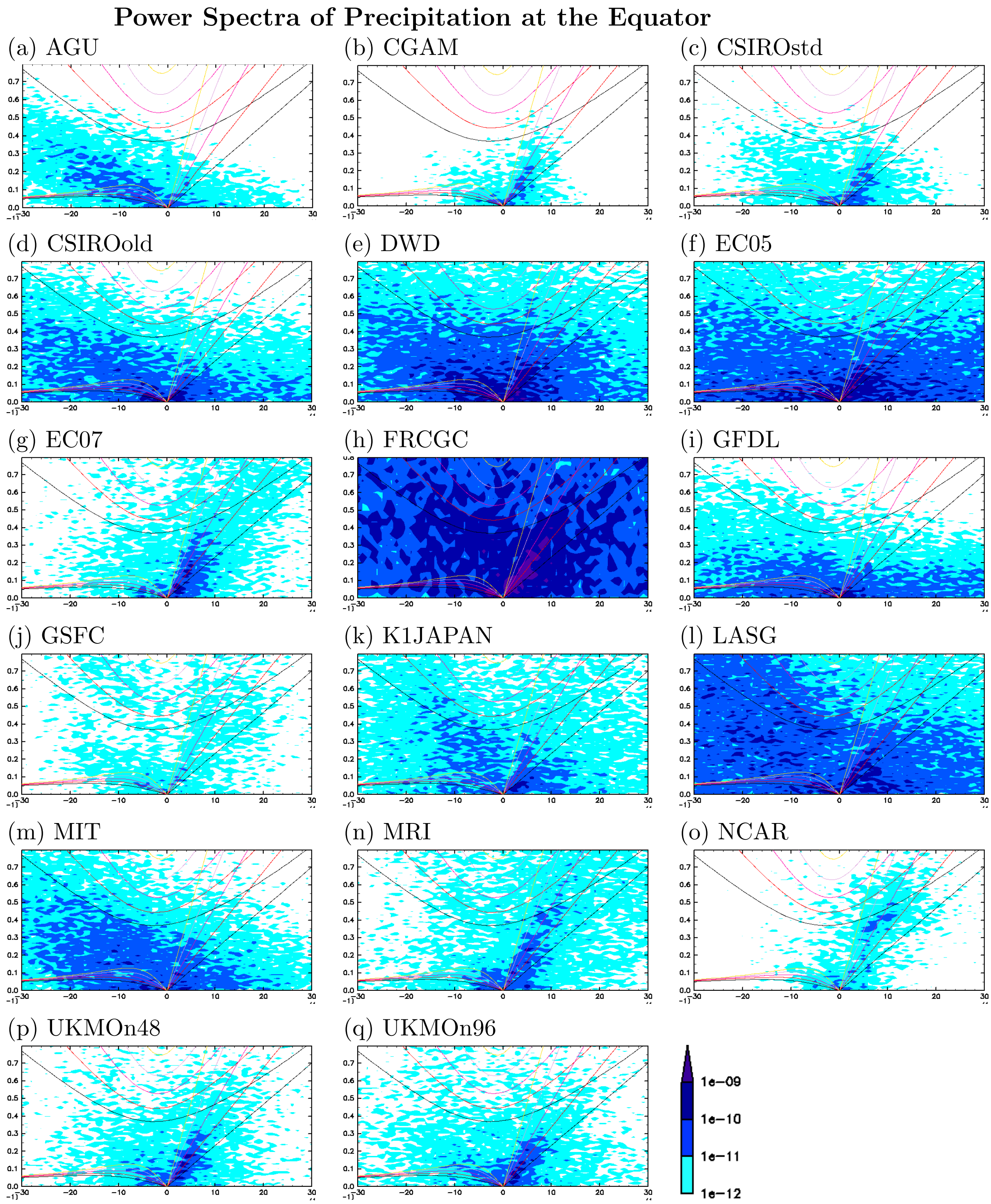

Fig. 4. Wavenumber-frequency spectra of power of precipitation at the equator. Unit is $kg^2 \cdot m^{-4} \cdot s^{-2}$.

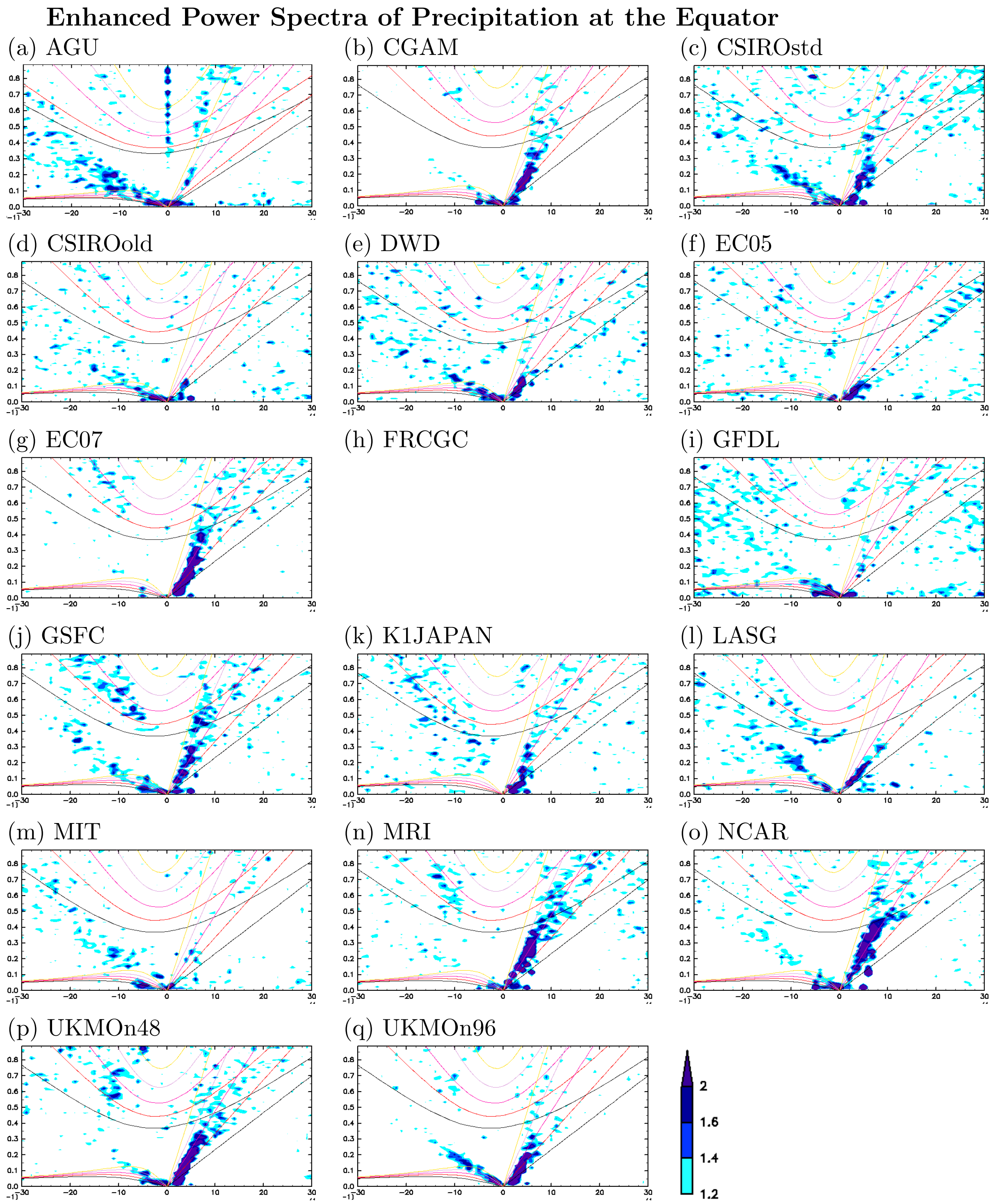

Fig. 5. Wavenumber-frequency diagrams of the intensity of power of precipitation at the equator relative to the background level (see text). The figure for FRCGC is not produced.

(a)

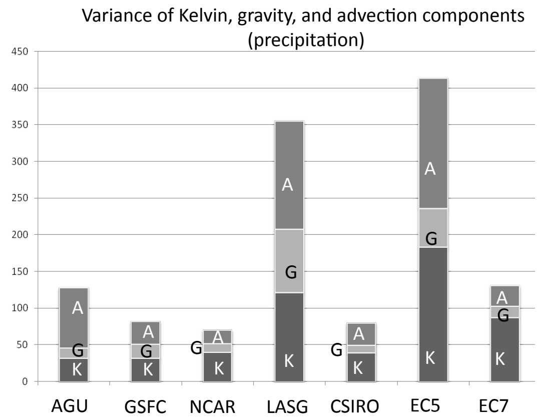

(b)

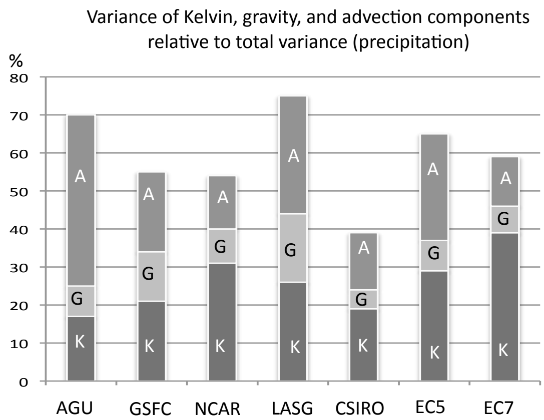

Fig. 6. (a) Variance of precipitation along equator for K, WIG,and AD. (b) Same as a, but for the values normalized by the total variance of precipitation.

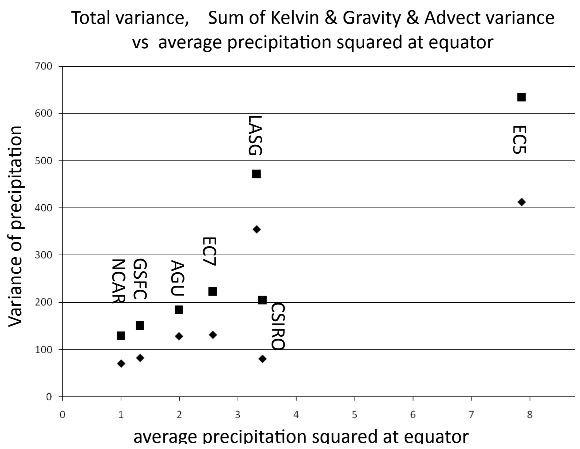

Fig. 7. Scattering diagram showing the relationship betweeb the average precipitation squared and total variance of precipitation along equator, the diamonds for the sum of K, WIG, AD components, and the squares for the total variance.

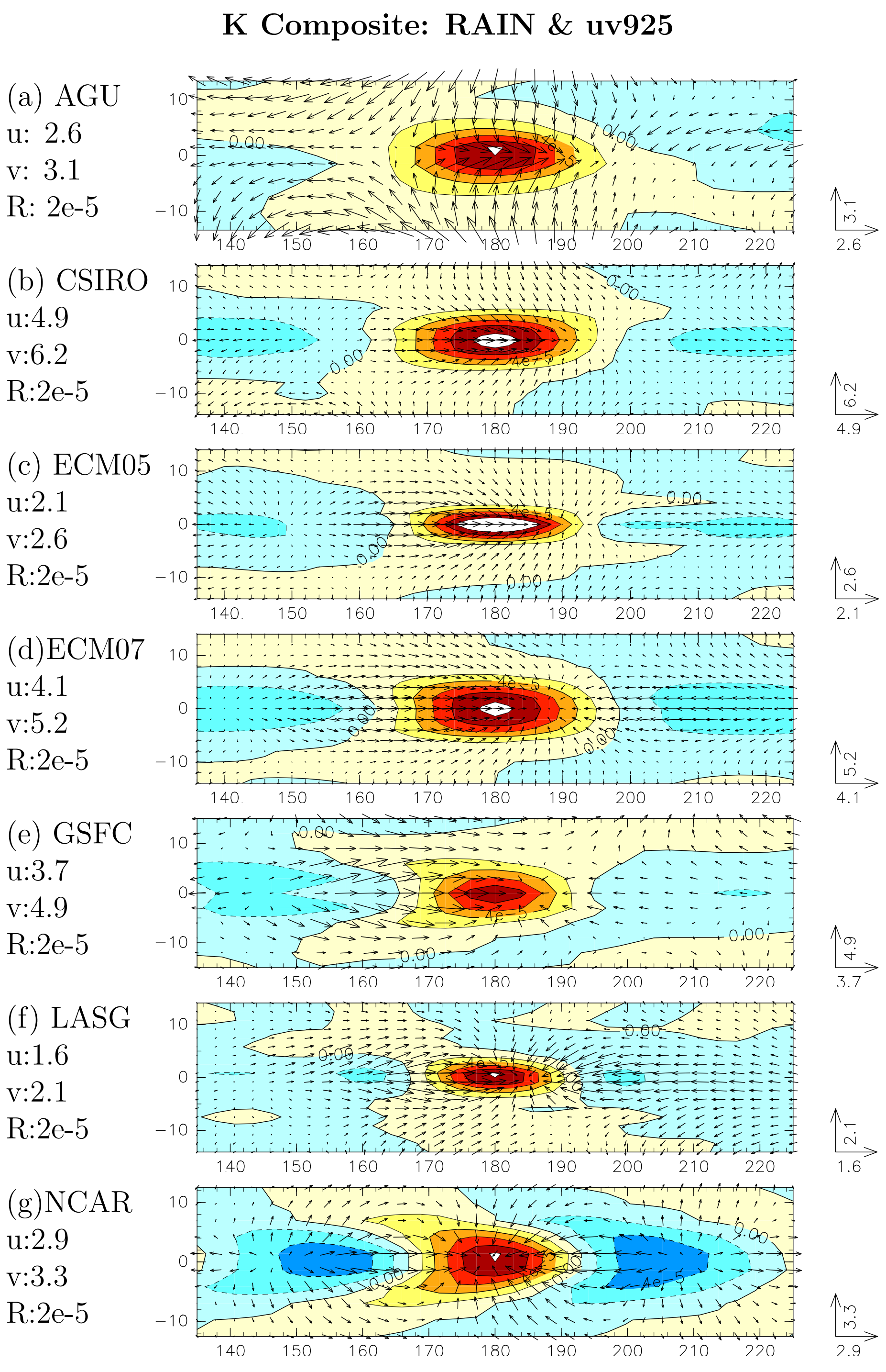

Fig. 8. Horizontal structure of Kelvin filtered composite showing anomaly of precipitation and wind vector at 925hPa. The velocity scales for the unit vector and the contour interval for precipitation are given to the left in [m/s] and [Kg/s].

K Composite : ϕuv850

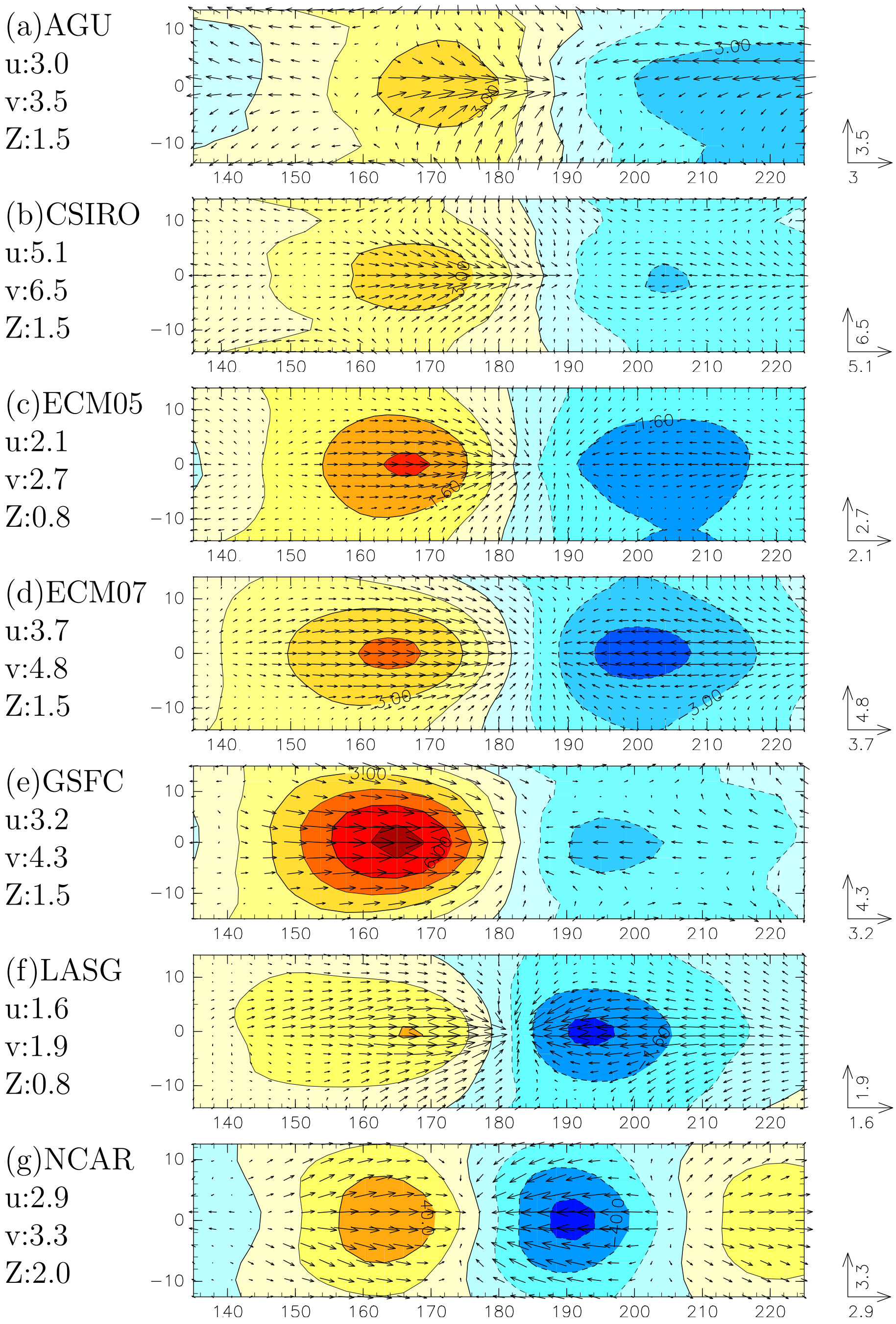

Fig. 9. Horizontal structure of Kelvin filtered composite showing anomaly of geopotential height and wind vector at 850hPa. The velocity scales for the unit vector and the contour interval for geopotential heifht are given to the left in [m/s] and [m].

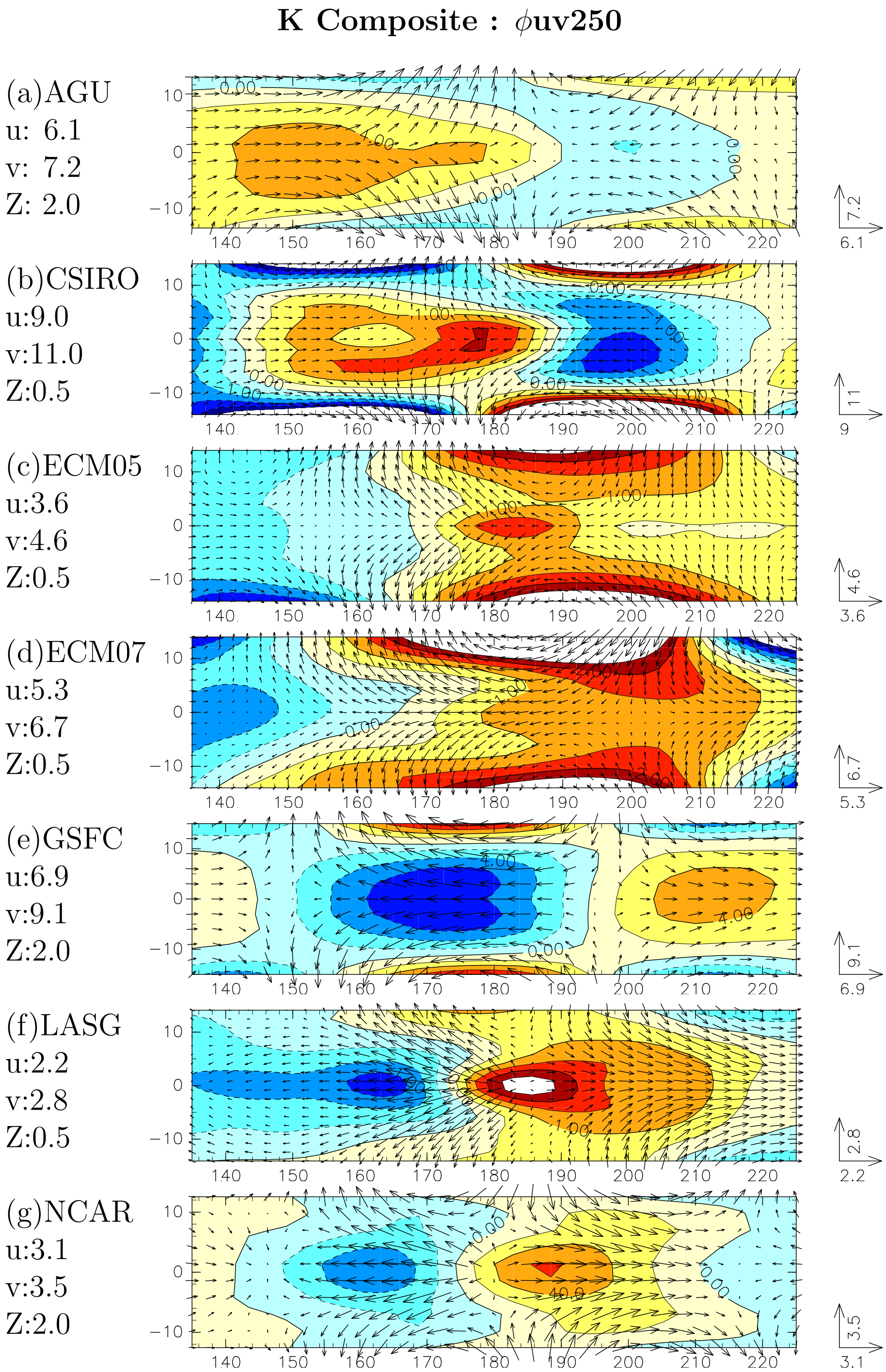

Fig. 10. Horizontal structure of Kelvin filtered composite showing anomaly of geopotential height and wind vector at 250hPa. The velocity scales for the unit vector and the contour interval for geopotential height are given to the left in [m/s] and [m].

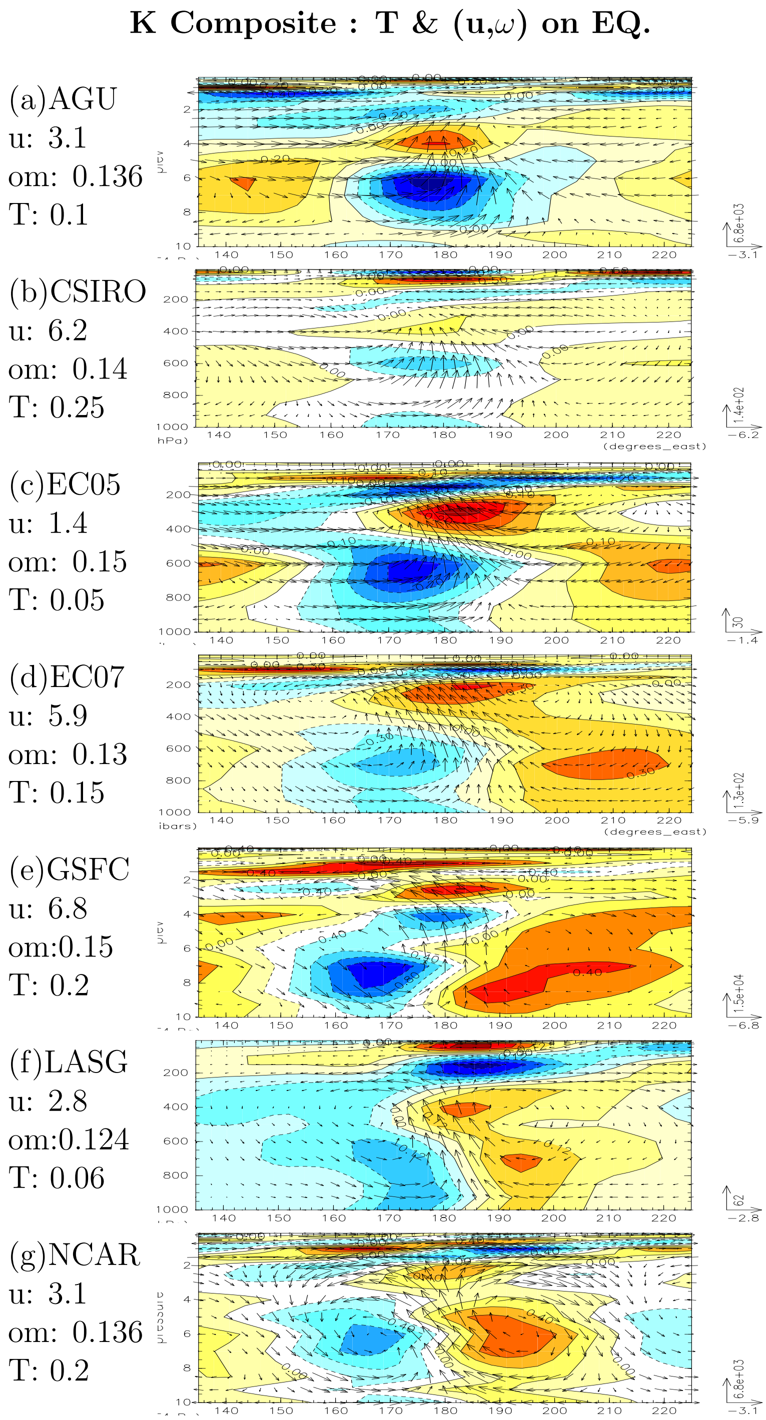

Fig. 11. Vertical structure of Kelvin filtered composite showing anomaly of temperature, zonal wind and p-vertical velocity along the equator. The velocity scales for the unit vector and the contour interval for temperature are given to the left in [m/s],[Pa/s],and [K].

K Composite : Q & (u,ω) on EQ.

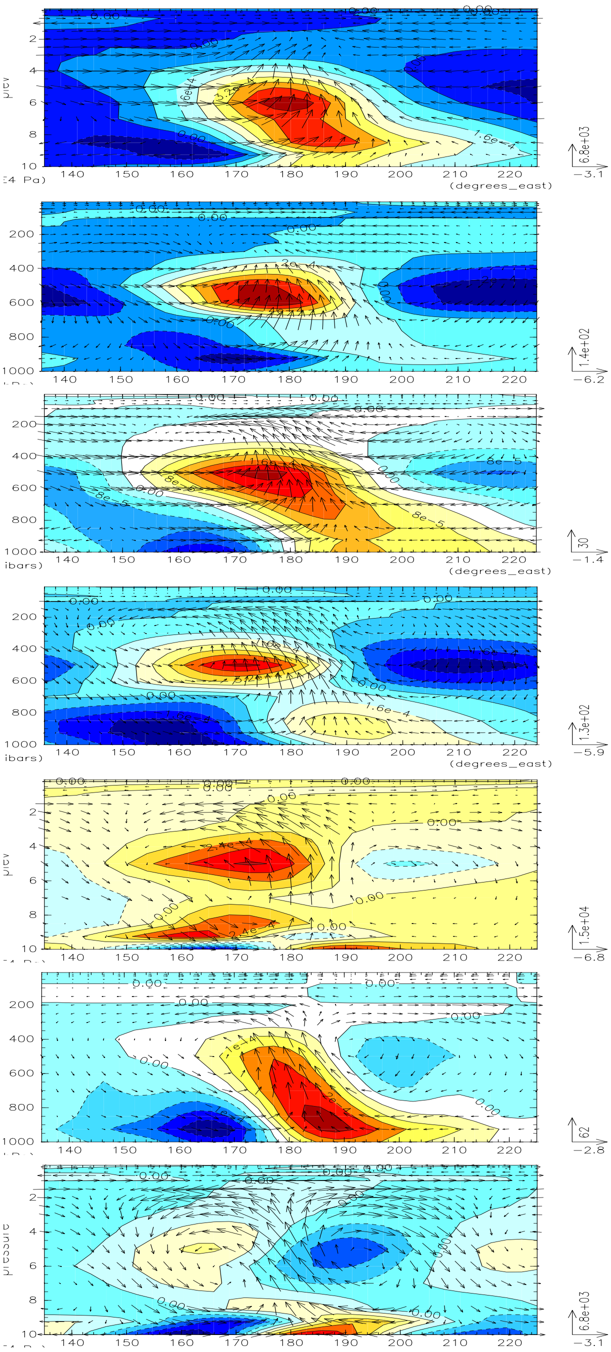

Fig. 12. Vertical structure of Kelvin filtered composite showing anomaly of mixing ratio, zonal wind and p-vertical velocity along the equator. The velocity scales for the unit vector and the contour interval for mixing ratio are given to the left in [m/s],[Pa/s],and [kg/kg].

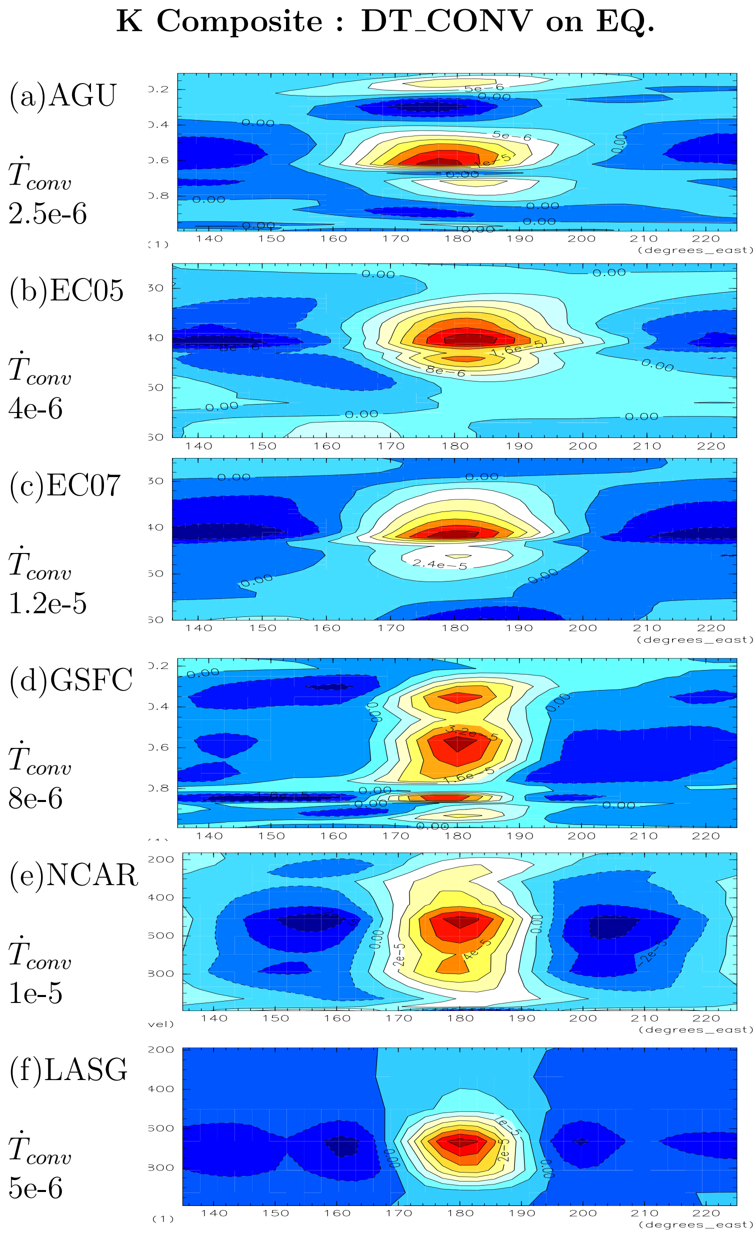

Fig. 13. Vertical structure of Kelvin filtered composite showing anomaly of convective heating. The contour interval are given to the left in [K/s].

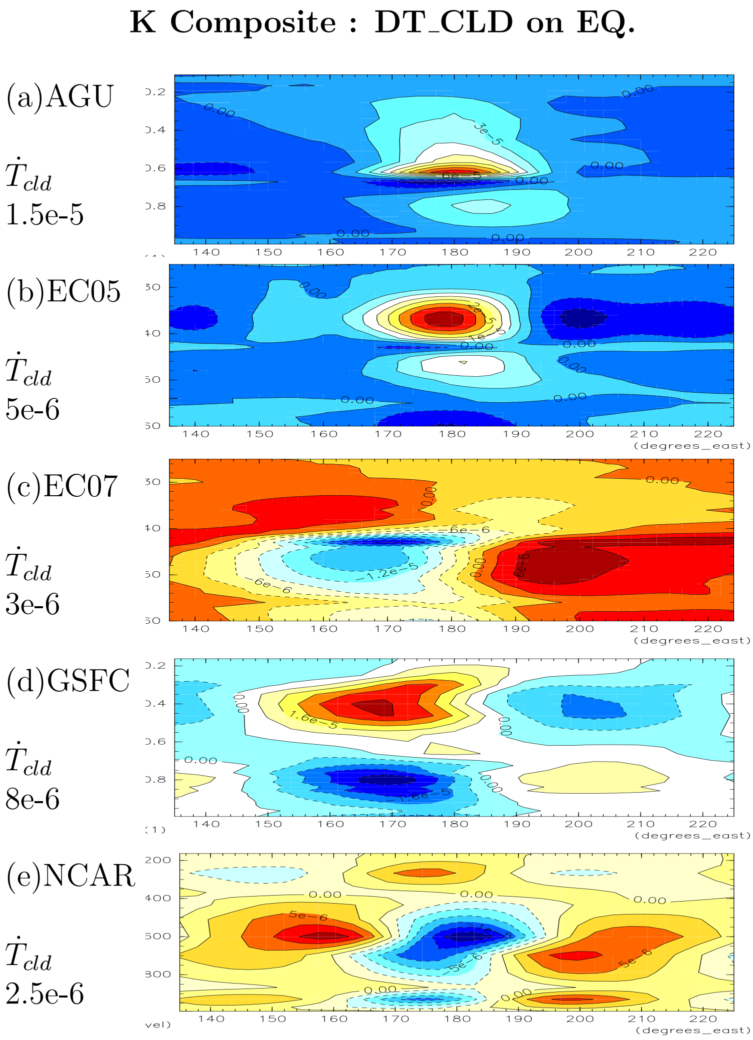

Fig. 14. Vertical structure of Kelvin filtered composite showing anomaly of non-convective heating. The contour interval are given to the left in [K/s].

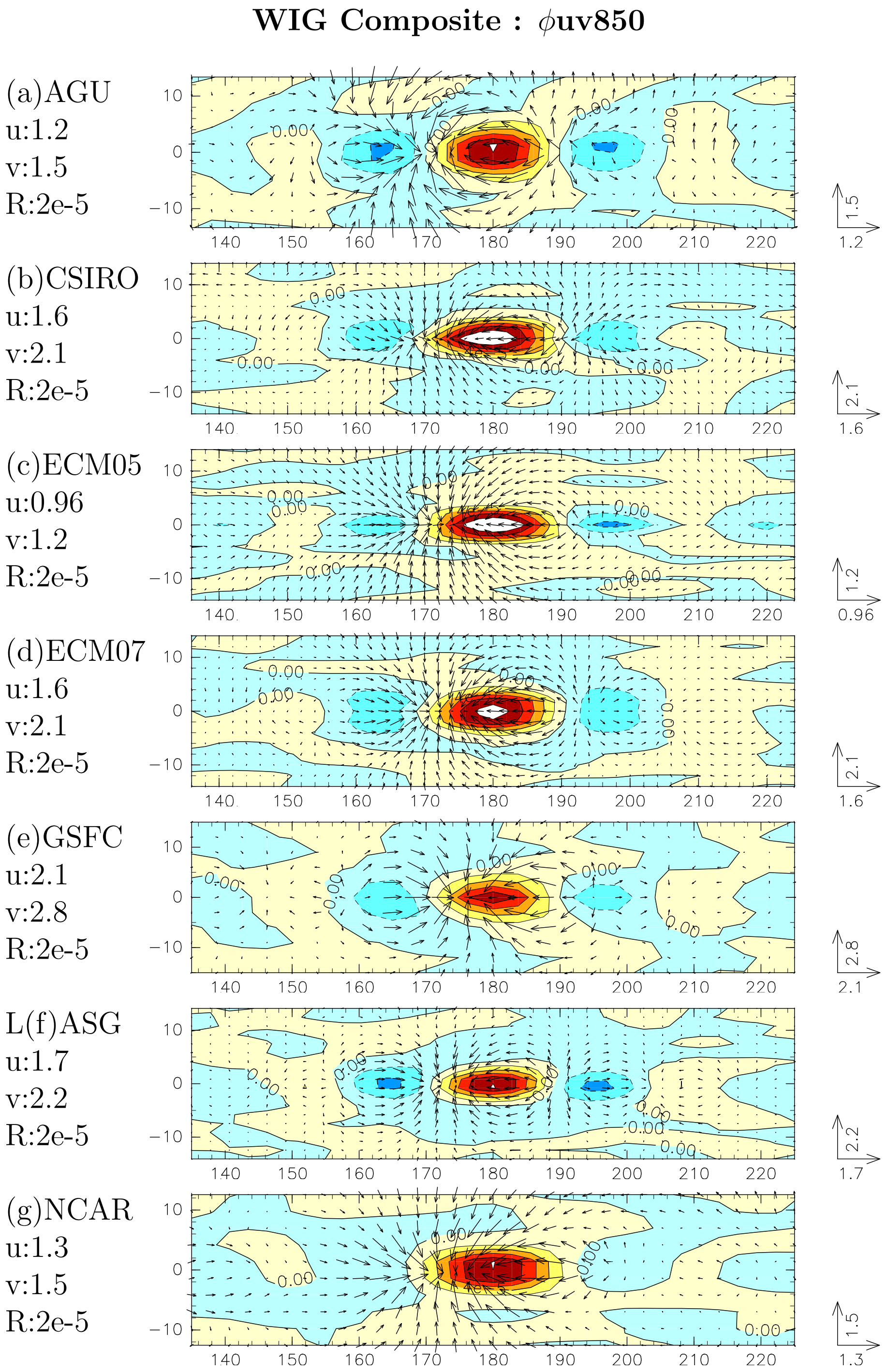

Fig. 15. Horizontal structure of WIG filtered composite showing anomaly of precipitation and wind vector at 925hPa. The velocity scales for the unit vector and the contour interval for precipitation are given to the left in [m/s] and [Kg/s].

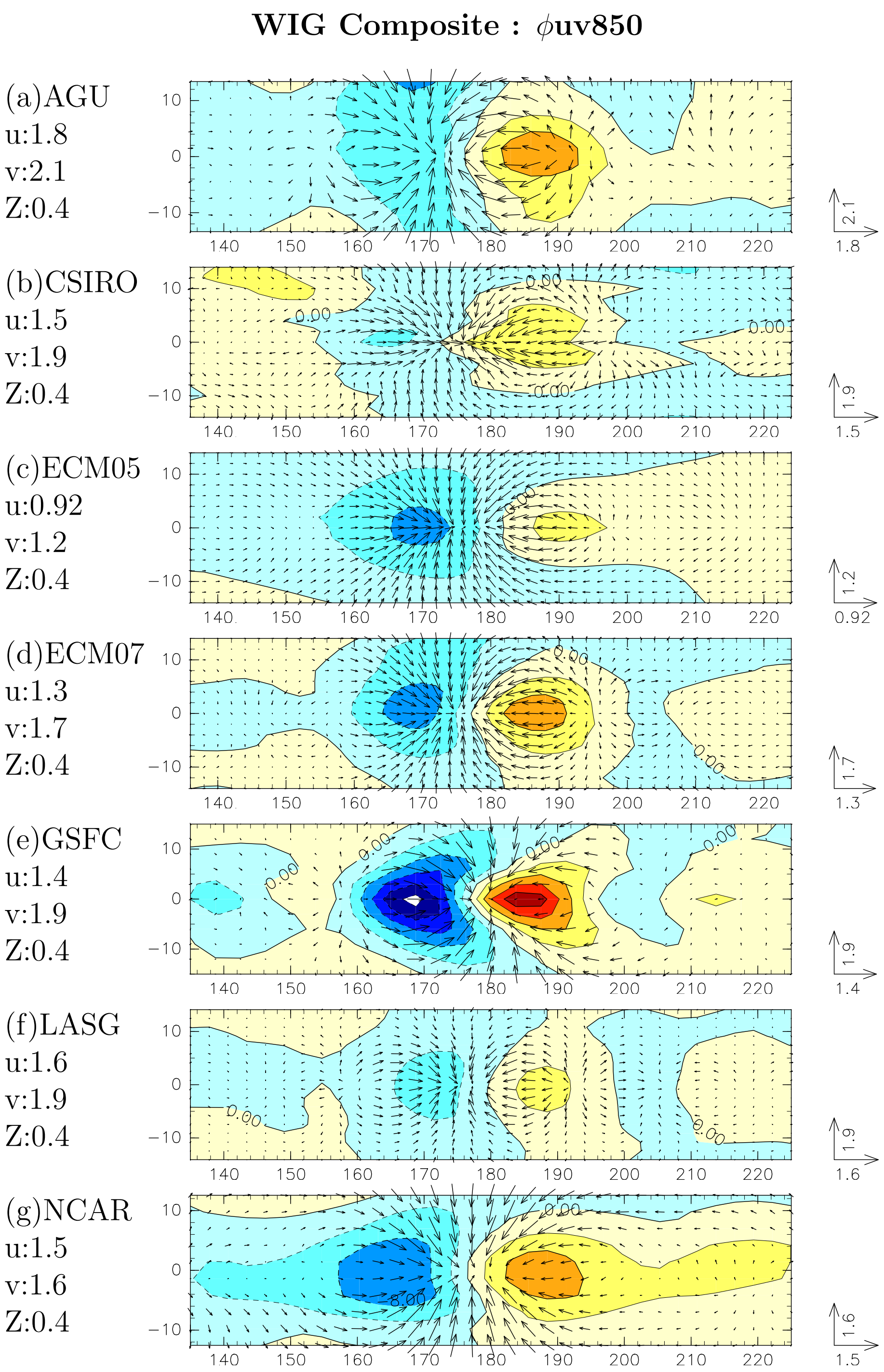

Fig. 16. Horizontal structure of WIG filtered composite showing anomaly of geopotential height and wind vector at 850hPa. The velocity scales for the unit vector and the contour interval for geopotential heifht are given to the left in [m/s] and [m].

WIG Composite : ϕuv250

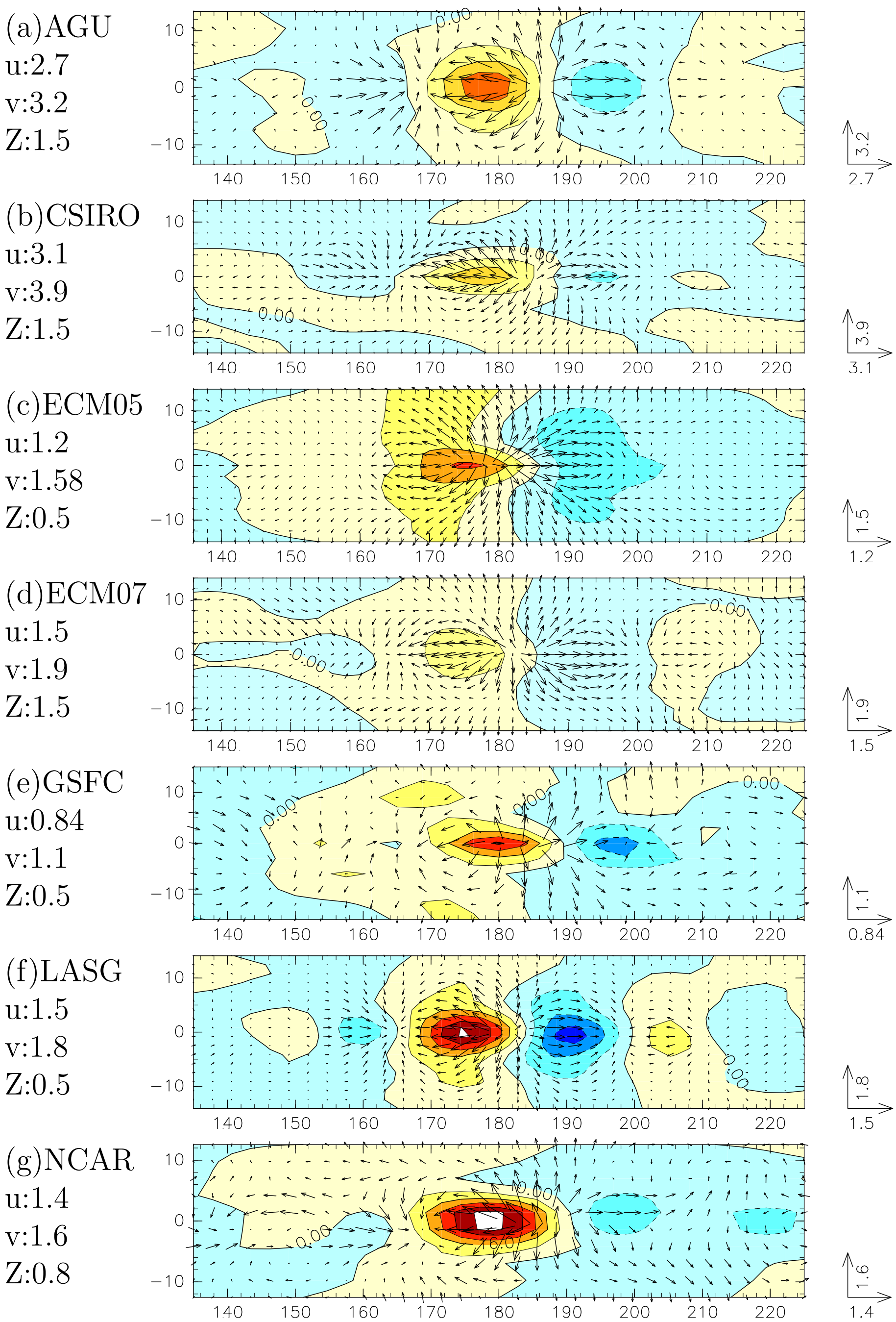

Fig. 17. Horizontal structure of WIG filtered composite showing anomaly of geopotential height and wind vector at 250hPa. The velocity scales for the unit vector and the contour interval for geopotential heifht are given to the left in [m/s] and [m].

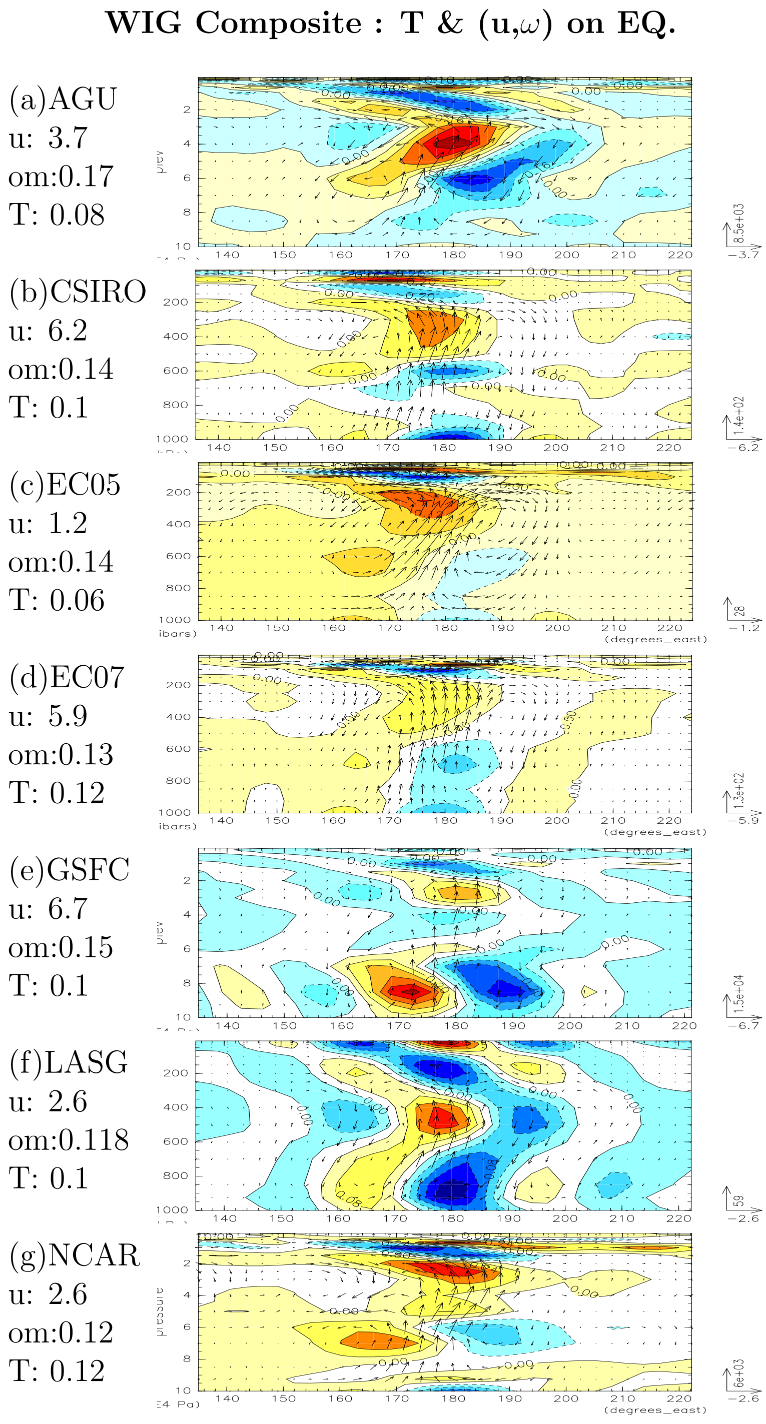

Fig. 18. Horizontal structure of WIG filtered composite showing anomaly of geopotential height and wind vector at 250hPa. The velocity scales for the unit vector and the contour interval for geopotential height are given to the left in [m/s] and [m].

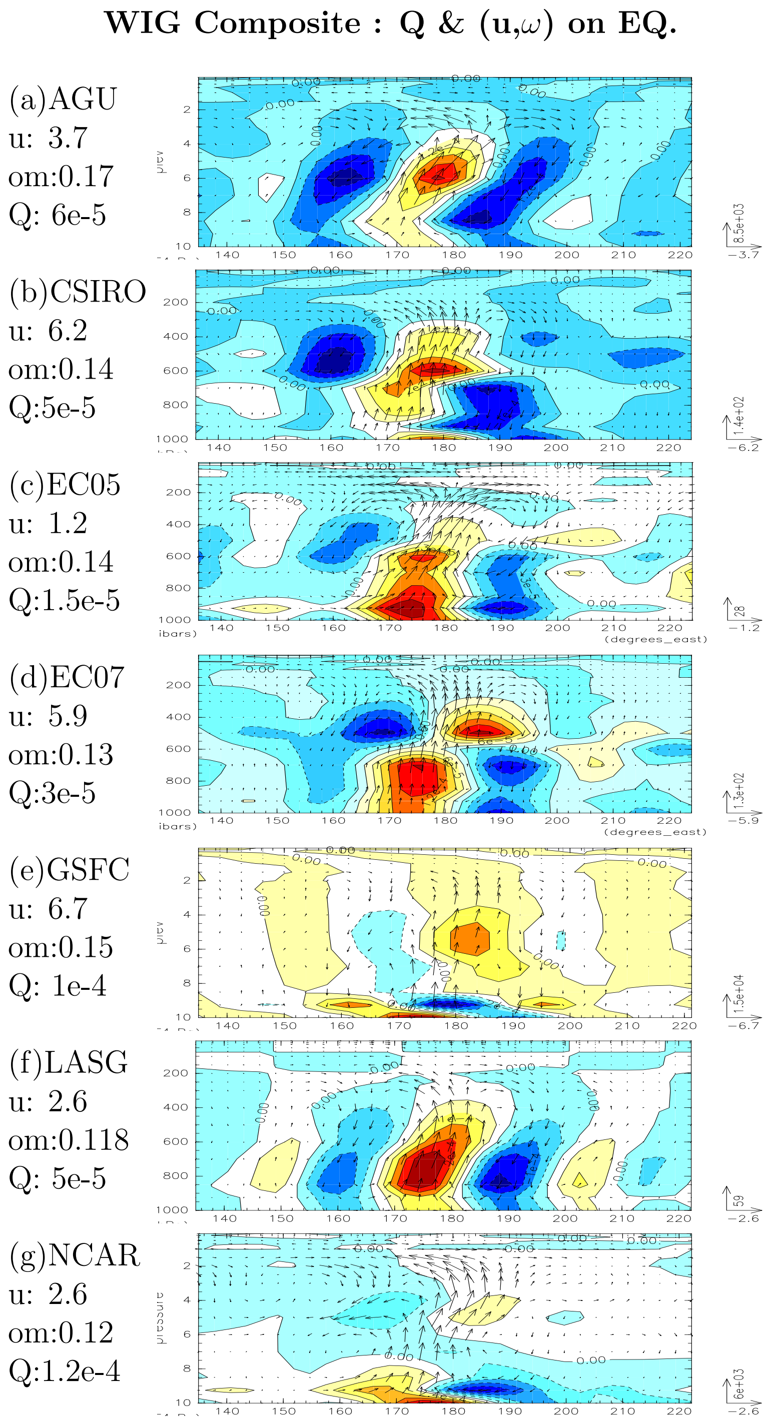

Fig. 19. Vertical structure of WIG filtered composite showing anomaly of temperature, zonal wind and p-vertical velocity along the equator. The velocity scales for the unit vector and the contour interval for temperature are given to the left in [m/s],[Pa/s],and [K].

WIG Composite : DT_CONV on EQ.

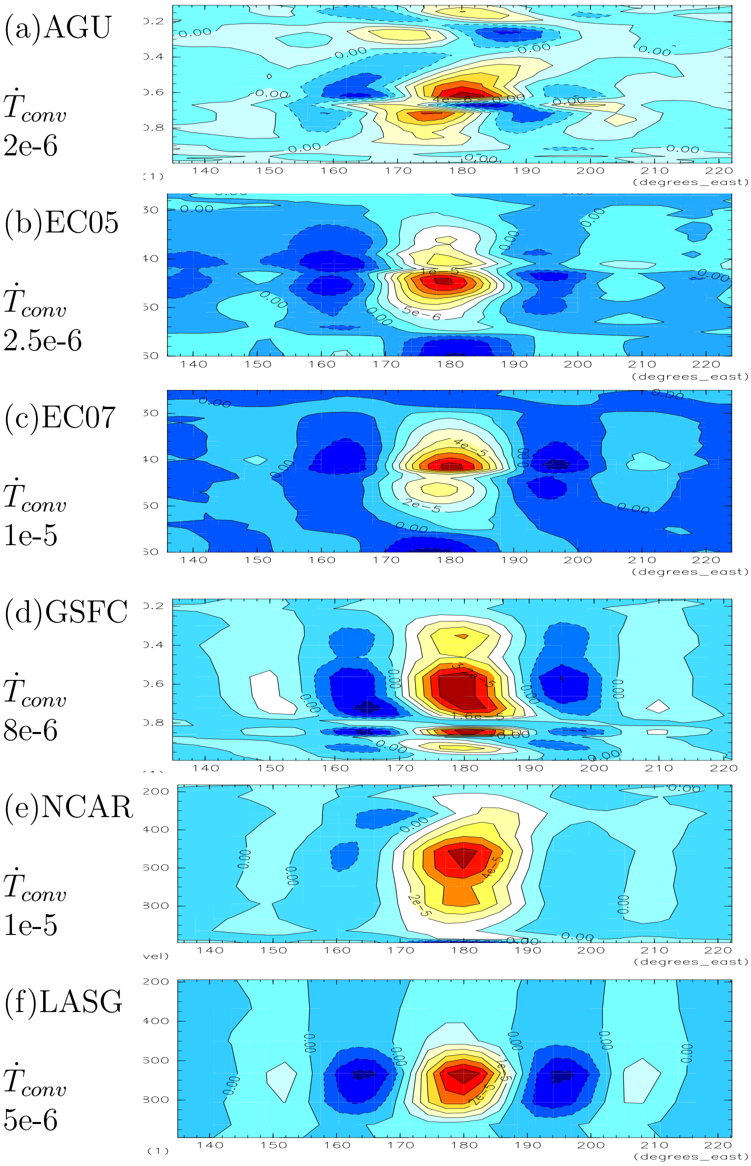

Fig. 20. Vertical structure of WIG filtered composite showing anomaly of convective heating. The contour interval are given to the left in [K/s].

WIG Composite : DT_CLD on EQ.

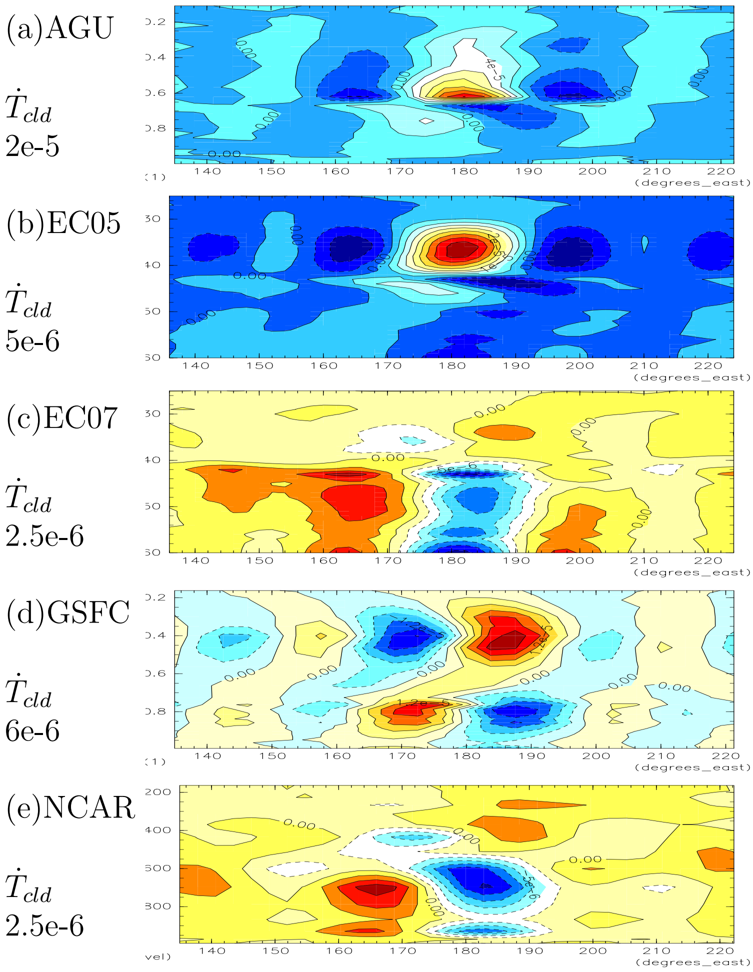

Fig. 21. Vertical structure of WIG filtered composite showing anomaly of non-convective heating. The contour interval are given to the left in [K/s].

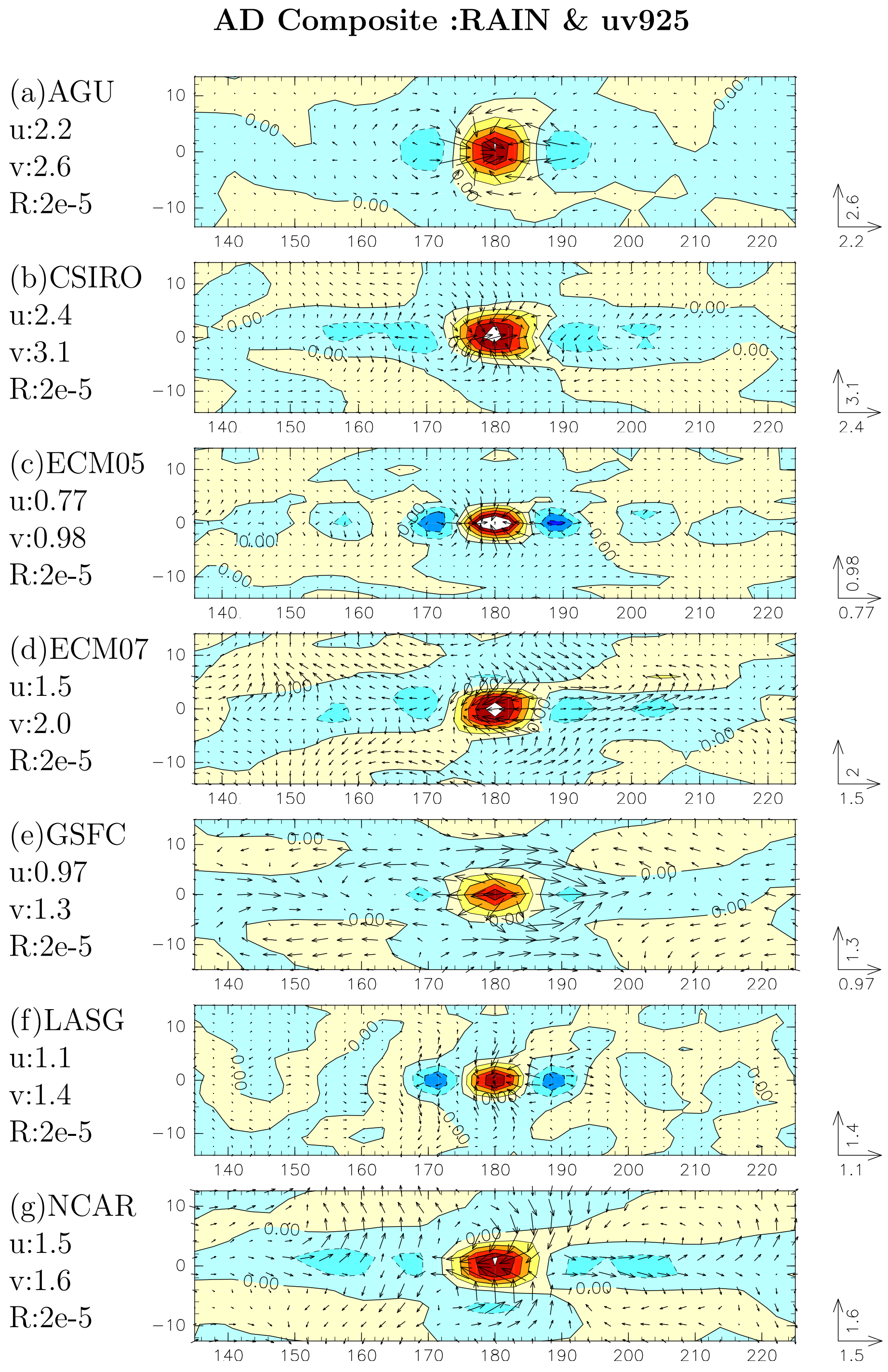

Fig. 22. Horizontal structure of AD filtered composite showing anomaly of precipitation and wind vector at 925hPa. The velocity scales for the unit vector and the contour interval for precipitation are given to the left in [m/s] and [Kg/s].

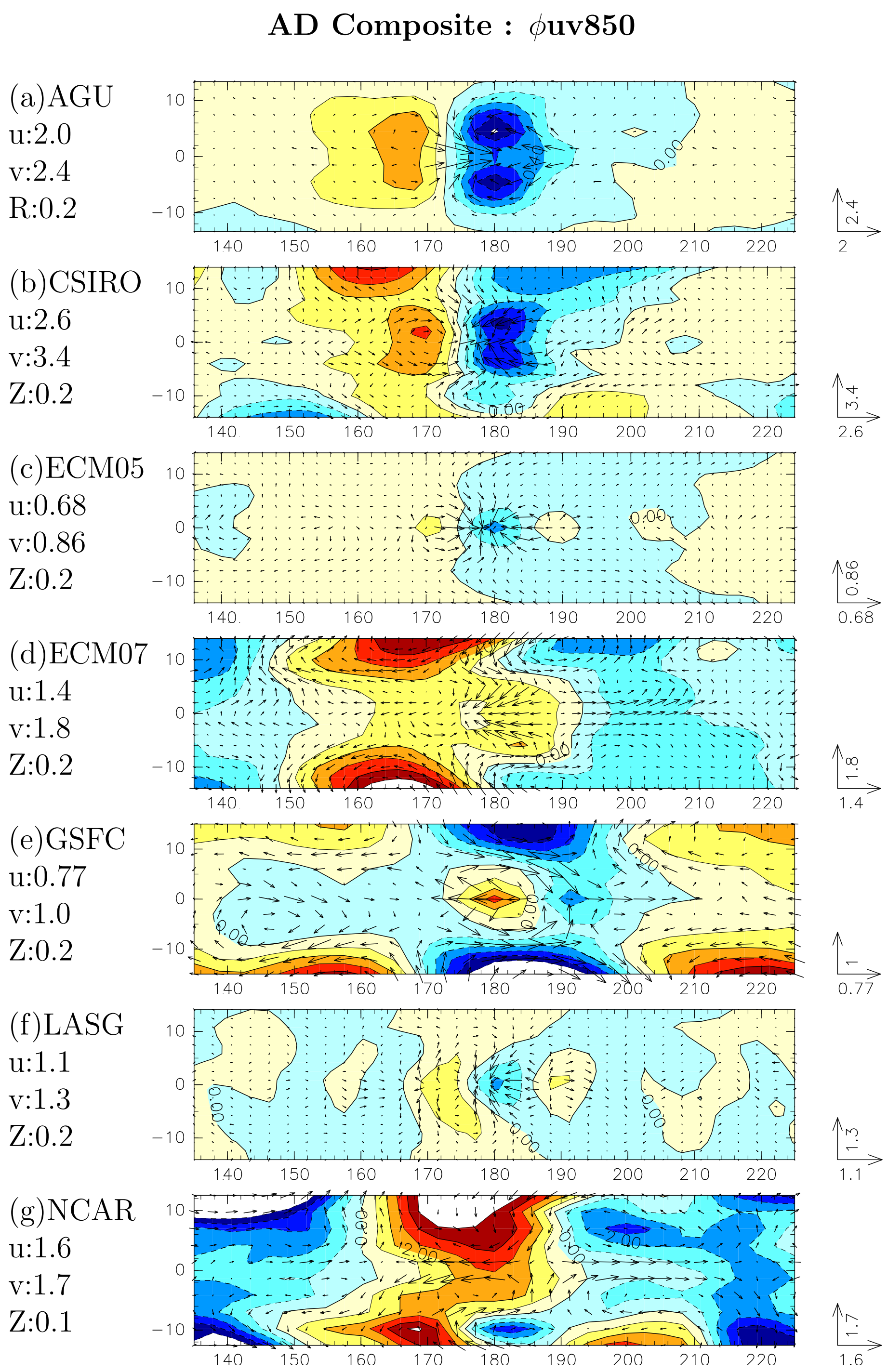

Fig. 23. Horizontal structure of AD filtered composite showing anomaly of geopotential height and wind vector at 850hPa. The velocity scales for the unit vector and the contour interval for geopotential heifht are given to the left in [m/s] and [m].

AD Composite : ϕuv250

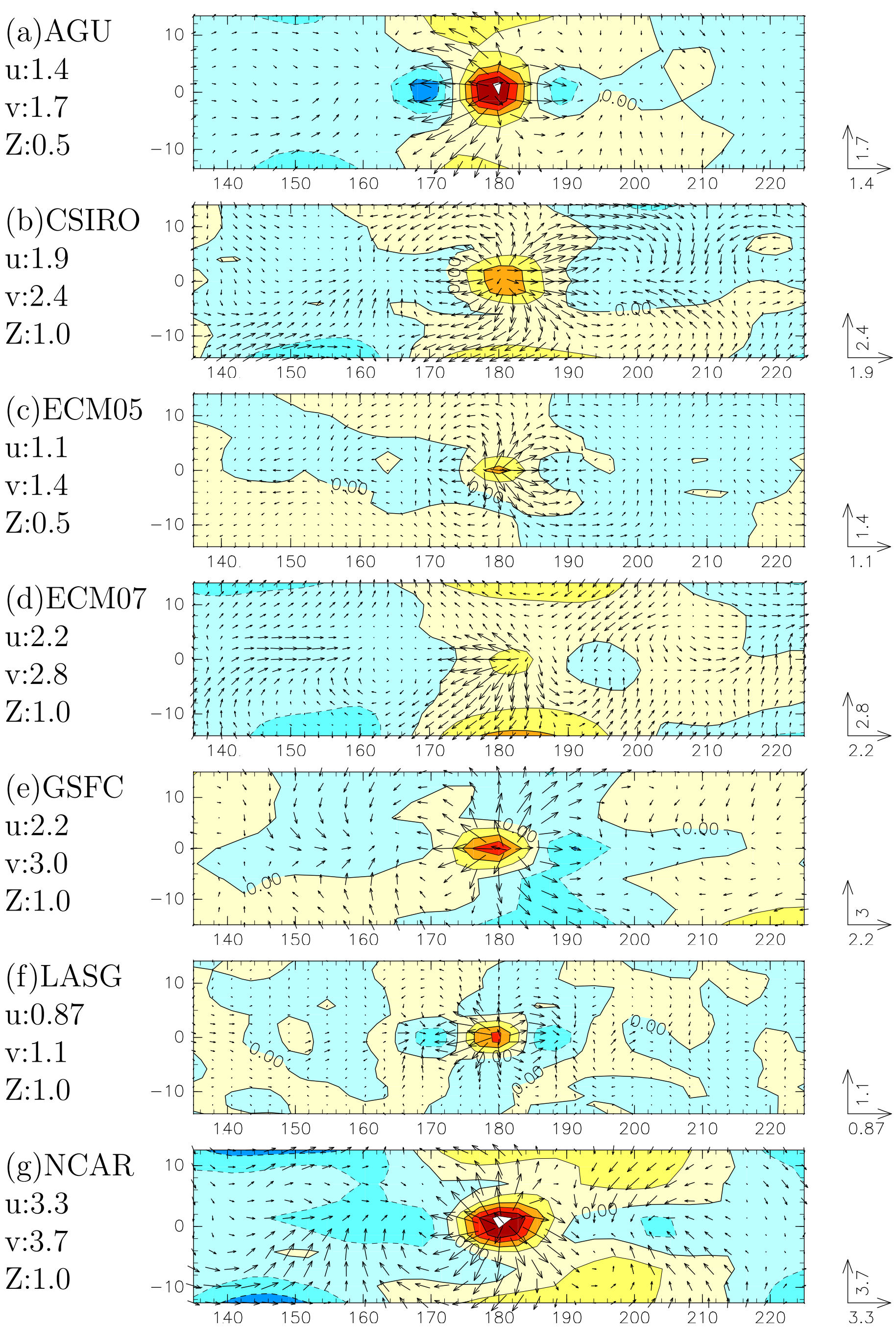

Fig. 24. Horizontal structure of AD filtered composite showing anomaly of geopotential height and wind vector at 250hPa. The velocity scales for the unit vector and the contour interval for geopotential height are given to the left in [m/s] and [m].

AD Composite : T & (u,ω) on EQ.

(a)AGU
u:3.3
om:0.15
T:0.04

(b)CSIRO
u:6.4
om:0.14
T:0.05

(c)EC05
u:1.3
om:0.15
T:0.015

(d)EC07
u:6.5
om:0.15
T:0.05

(e)GSFC
u:12.0
om:0.26
T:0.04

(f)LASG
u:2.4
om:0.108
T:0.04

(g)NCAR
u:4.3
om:0.198
T:0.05

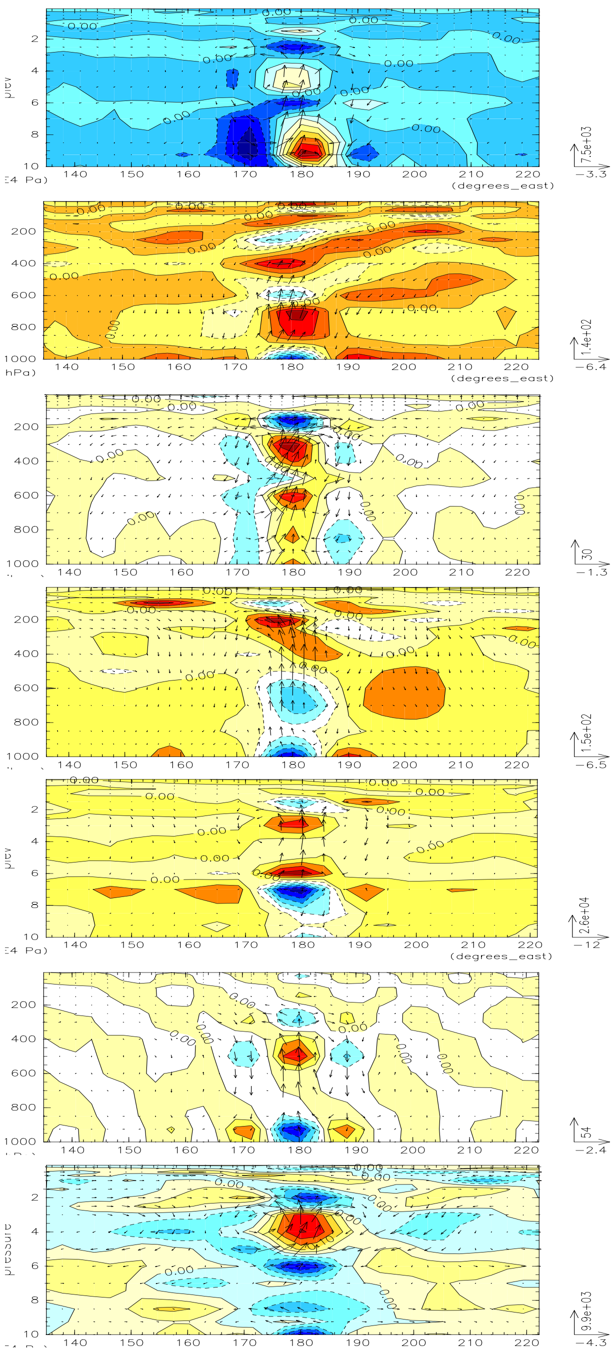

Fig. 25. Vertical structure of AD filtered composite showing anomaly of temperature, zonal wind and p-vertical velocity along the equator. The velocity scales for the unit vector and the contour interval for temperature are given to the left in [m/s],[Pa/s],and [K].

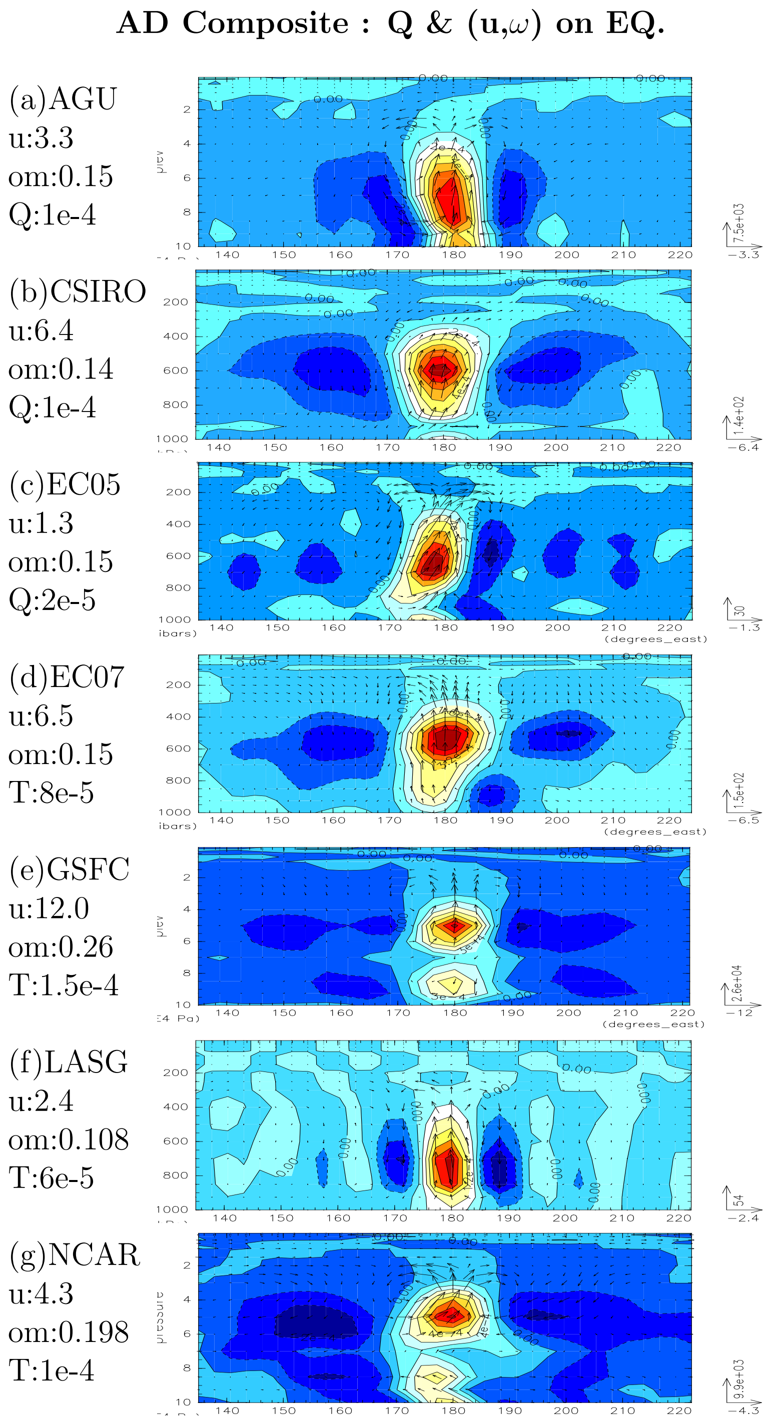

Fig. 26. Vertical structure of AD filtered composite showing anomaly of mixing ratio, zonal wind and p-vertical velocity along the equator. The velocity scales for the unit vector and the contour interval for mixing ratio are given to the left in [m/s],[Pa/s],and [kg/kg].

AD Composite : DT_CONV on EQ.

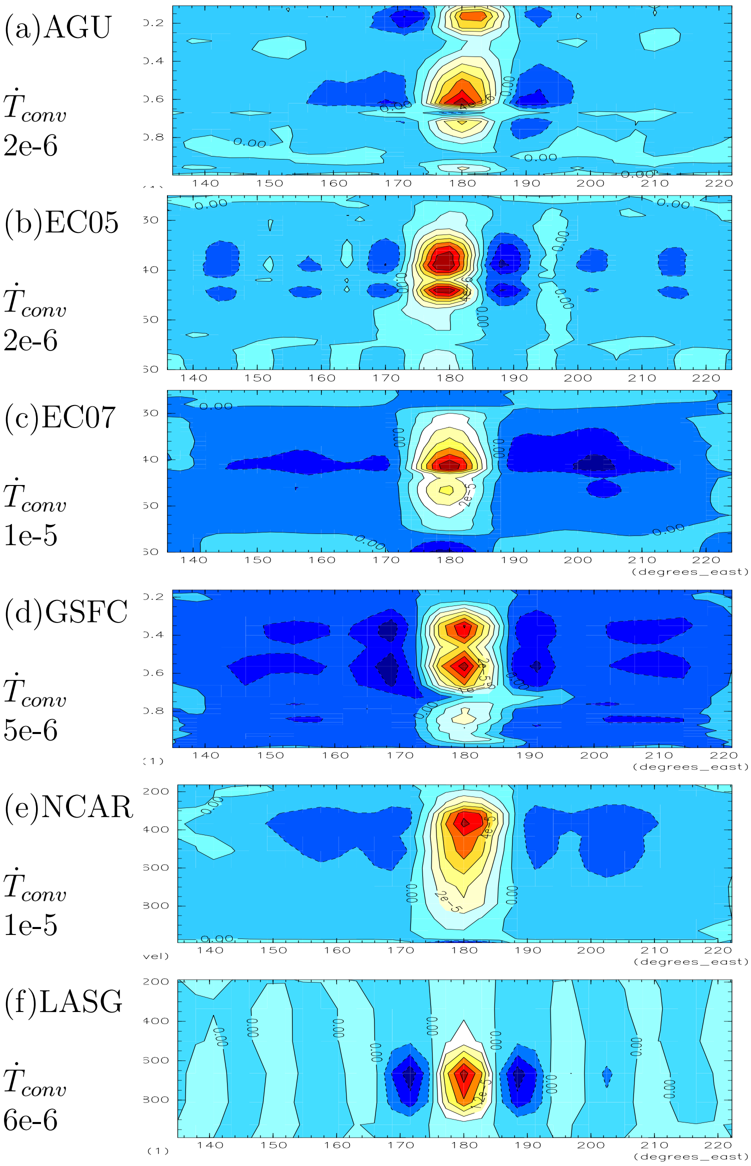

Fig. 27. Vertical structure of AD filtered composite showing anomaly of convective heating. The contour interval are given to the left in [K/s].

AD Composite : DT_CLD on EQ.

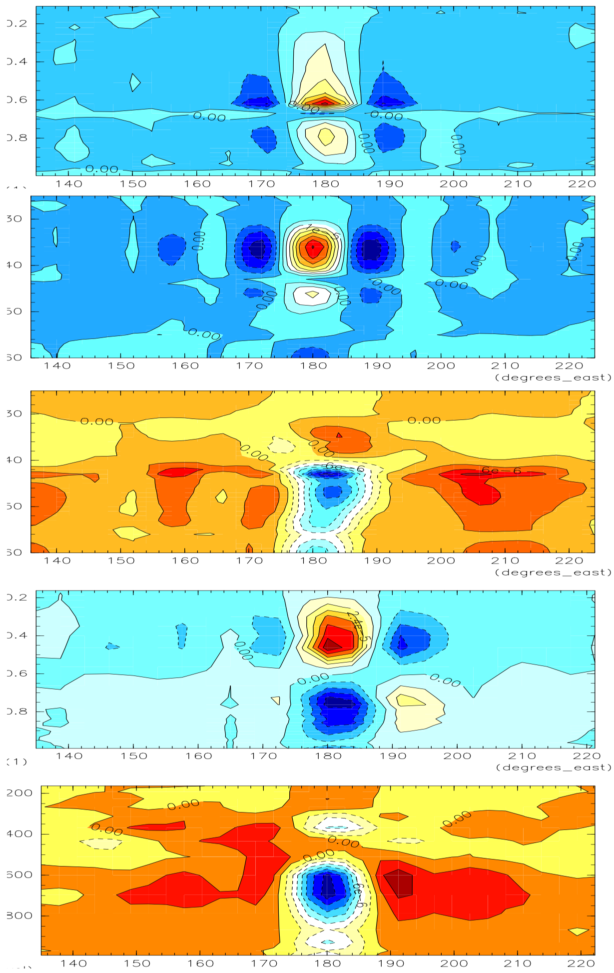

Fig. 28. Vertical structure of AD filtered composite showing anomaly of non-convective heating. The contour interval are given to the left in [K/s].

List of Tables

Table 1. Participating models

GROUP SYMBOL	MODEL	HORIZONTAL RESOLUTION	NO.OF LEVELS	DEEP CONVECTION	COM-POSITE
AGU	AFES	T39	48	Emanuel	yes
CGAM	HadAM3	3.75° x 2.5°	30	Gregory-Rawntree	-
CSIROstd	CCAM-05e	∼210km	18	McGregor	yes
CSIROold	CCAM-05a	∼210km	18	McGregor	-
DWD	GME	∼1°	31	Tiedtke	-
EC05	IFS cy29r2	T159	60	Bechtold et al 2004	yes
EC07	IFS cy32r3	T159	60	Bechtold et al 2008	yes
FRCGC	NICAM	∼7km	54	None	-
GFDL	AM2.1	2.5° x 2°	24	RAS	-
GSFC	NSIPP-1	3.75° x 3°	34	RAS	yes
K1JAPAN	CCSR/NIES 5.7	T42	20	Pan-Randall	-
LASG	SAMIL	R42	9	Manabe	yes
MIT	MIT-GCM	∼280km	40	RAS	-
MRI	MRI/JMA98	T42	30	Randall-Pan	-
NCAR	CCSM-CAM3	T42	26	Zhang-McFarlane	yes
UKMOn48	pre-HadGAM1	3.75° x 2.5°	38	Gregory 1999	-
UKMOn96	pre-HadGAM1	1.875° x 1.25°	38	Gregory 1999	-